PNAS
www.pnas.org

# Supplementary Information for

## Understanding the co-evolution of mask-wearing and epidemics : a network perspective

**Zirou Qiu, Baltazar Espinoza, Vítor V. Vasconcelos, Chen Chen, Sara M. Constantino, Stefani A. Crabtree, Luojun Yang, Anil Vullikanti, Jiangzhuo Chen, Jörgen Weibull, Kaushik Basu, Avinash Dixit, Simon A. Levin, Madhav V. Marathe**

**Zirou Qiu, Madhav V. Marathe, Simon A. Levin.**
**E-mail: {zq5au, marathe}@virginia.edu, slevin@princeton.edu**

**This PDF file includes:**

In the Supplementary document, we provide $(i)$ formal definition of the network model and the ODE model; $(ii)$ an overview of the existing work on complex contagions, the threshold model and multi-contagion frameworks; $(iii)$ Methodology in selecting baseline parameters; $(iv)$ Results for the robustness of the critical transitions for the network model; $(v)$ Additional results for the ODE model.

**Reproducibility:** The analysis code are publicly available at:
https://github.com/BridgelessAlexQiu/Mask-Disease-Multilayer.

## The Network Model of Dueling Contagions

Let $\mathcal{A} = \{a_1, a_2\}$ be the set of two contagions in which $a_1$ is the social contagion *mask-wearing*, and $a_2$ is a *disease*. We model the dissemination of the dueling contagions using a *graphical dynamical system* (1). Specifically, a graphical dynamical system $\mathcal{S}$ is defined as a pair $(\mathcal{M}, \mathcal{F})$ where

$(i)$ $\mathcal{M} = \{G_1, G_2\}$ is a two-layer network for which $G_1 = (V, E_1)$ is the the social layer, and $G_2 = (V, E_2)$ is the the biological layer. Layers $G_1$ and $G_2$ are defined over the **same** synthetic population $V$ of size $n$, and they differ by the set of edges. The contagion $a_i$ spreads only on $G_i$, $i = 1, 2$.

$(ii)$ $\mathcal{F} = \{f_{i,j} : a_i \in \mathcal{A}, v_j \in V\}$ is a collection of functions for which $f_{i,j}$ is the **local transition function** of vertex $v_j \in V, 1 \leq j \leq n$ for the contagion $a_i$, $i = 1, 2$. In general, $f_{i,j}$ specifies how $v_j$ updates its state for the contagion $a_i$.

An individual is associated with two states: $(i)$ a binary *social* state which indicates his/her decision in mask-wearing (i.e., state `M` represents wearing a mask, and state `NM` represents not wearing a mask), and $(ii)$ a *disease* state from $\{\texttt{S}, \texttt{I}, \texttt{R}\}$. At each time step, all individuals update their social and biological states *synchronously*. In the following sections, we define the local functions (i.e., update rules) for the social contagion and the biological contagion.

**Update rules for the social contagion.** The dynamics of the social contagion $a_1$ is captured by the threshold model (2). Specifically, we consider the following three factors in triggering an individual $v$ to wear a mask at time* $t > 1$:

$(i)$ *Peer pressure:* Let $\psi_1^{(t-1)}(v) \in [0, 1]$ be the fraction of $v$'s neighbors in $G_1$ who wear masks at time $t - 1$.

$(ii)$ *Fear:* Let $\psi_2^{(t-1)} \in [0, 1]$ be the fraction of infected individuals by the disease at time $t - 1$.

$(iii)$ *Prosociality:* Let $x(v) \in \{0, 1\}$ be an indicator random variable, for which $x(v) = 0$ if $v$ is not prosocial, and $x(v) = 1$ if $v$ is prosocial. Note that $x(v)$ is an initial condition of $v$ that does not change with time.

In addition, an individual $v$ has two thresholds defined as follows:

$(i)$ *Sensitivity to peer pressure*: Let $\tau_1(v) \in [0, 1]$ be the peer pressure threshold such that $v$ chooses to a mask at time $t$ if $\psi_1^{(t-1)}(v) \geq \tau_1(v)$, that is, the fraction of the $v$'s mask-wearing neighbors at time $t - 1$ is at least $\tau_1(v)$.

$(ii)$ *Fear for the disease:* Let $\tau_2(v) \in [0, 1]$ be the fear threshold such that $v$ chooses to a mask at time $t$ if $\psi_2^{(t-1)} \geq \tau_2(v)$, that is, the fraction of the overall infections is at least $\tau_2(v)$.

At each time step $t$, $t > 1$, an individual $v$ chooses to wear a mask if and only if at least one of the following three conditions is satisfied: $(i)$ $\psi_1^{(t-1)}(v) \geq \tau_1(v)$, $(ii)$ $\psi_2^{(t-1)} \geq \tau_2(v)$, or $(iii)$ $x(v) = 1$. In other words, an individual's mask-wearing behavior can be triggered by either peer pressure, fear, or prosociality. If none of the above conditions are satisfied, however, $v$ chooses not to wear a mask at time $t$. Please see the related work section for additional motivation of the model.

*We assume that the dynamics starts on time step 1.

**The local function.** To formally state the social dynamics, let $\mathbb{B}_1 = \{\texttt{M}, \texttt{NM}\}$ be the domain of the two states (i.e., `Mask` or `No-Mask`) for the social contagion $a_1$. The local function $f_{1,v}(v,t)$ computes the mask-wearing state of $v \in V$ at time step $t$. In particular,

$$f_{1,v}(v,t) = \begin{cases} \texttt{M} & \text{if } [\psi_1^{(t-1)}(v) \geq \tau_1(v)] \vee [\psi_2^{(t-1)} \geq \tau_2(v)] \vee x(v) \\ \texttt{NM} & \text{Otherwise} \end{cases}$$

where $\vee$ represent the logical OR function.

**Update rules for the disease.** The dynamics of disease $a_2$ adapts the `SIR` model under a simple extension for which it accounts for the effectiveness of mask-wearing in decreasing the disease infection rate. Let the disease *baseline transmission probability* $p \in [0,1]$ be the probability of infection for a susceptible individual $s$ in contact with an infected neighbor $i$, under the condition that **both $i$ and $s$ do not wear masks**. At a time step $t \geq 1$, if $i$ or $s$ wears a mask, however, the infection probability for $s$ decreases as follows

($i$) If only the susceptible vertex $s$ wears a mask at time $t$, $p$ is decreased to $\alpha p$, where $\alpha \in [0,1]$ is a discounting factor.

($ii$) If only the infected vertex $i$ wears a mask at time $t$, $p$ is decreased to $\beta p$, where $\beta \in [0,1]$ is a discounting factor.

($iii$) If both $i$ and $s$ wear masks at time $t$, the transmission probability becomes $\alpha\beta p$, where both discounting factors are applied.

**Table S1. Transmission probability under effectiveness of mask-wearing**

| State of *susceptible* | State of *infected* | Transmission Probability |
|---|---|---|
| NO-MASK | NO-MASK | $p$ |
| MASK | NO-MASK | $\alpha p$ |
| NO-MASK | MASK | $\beta p$ |
| MASK | MASK | $\alpha\beta p$ |

The parameters $\alpha$ and $\beta$ capture the effectiveness of masks. Note that $\alpha$, $\beta$, and $p$ are constants over the course of the pandemic.

**The local function.** To formally define the disease dynamics, let $\mathbb{B}_2 = \{\texttt{S}, \texttt{I}, \texttt{R}\}$ the set of disease states. The local function $f_{2,v}(v,t)$ is a probabilistic function that determines the state of $v \in V$ for $a_2$ at time step $t$. In particular,

($i$) If $v$ is susceptible at time $t-1$, $f_{2,v}(\cdot)$ captures the probabilistic process for infection. Given a susceptible vertex $v \in V$, let $d_1^{(t-1)}$ be the number of $v$'s mask-wearing infected neighbors in $G_2$, at time $t-1$. Let $d_2^{(t-1)}$ denote the number of $v$'s mask-free infected neighbors in $G_2$, at time $t-1$. Then the probability of $v$ gets infected at time $t$ is defined as

$$Pr(v \text{ gets infected}) = \begin{cases} 1 - [(1-\alpha\beta p)^{d_1^{(t-1)}} \cdot (1-\alpha p)^{d_2^{(t-1)}}] & \text{If } v \text{ wears a mask at time } t \\ 1 - [(1-\beta p)^{d_1^{(t-1)}} \cdot (1-p)^{d_2^{(t-1)}}] & \text{Otherwise} \end{cases}$$

($ii$) If $v$ is infected at time $t-1$, then $f_{2,v}(\cdot)$ captures the probabilistic process for recovery. Under each time step, each infected vertex recovers with a fixed probability $r \in [0,1]$, that is,

$$Pr(v \text{ recovers}) = r$$

($iii$) If $v$ is recovered, it remains recovered for all succeeding time steps.

## Related Work

**Complex contagions and threshold models.** Social contagions such as *mask-wearing* behavior, public opinions, and social norms can be broadly described as *complex contagions* whose adoptions require multiple sources of influence (3). Centola and Macy (3) first introduced the concept of complex contagions in 2007. Specifically, based on Watts and Strogatz's small-world network model (4), Centola and Macy showed that having long ties in the network could hinder the spread of complex contagions (3). Complex contagions have since been widely investigated in areas such as social science (5, 6), public health (7, 8), and political science (9, 10). We refer reader to the work by Guilbeault et al. (11) for a detailed review.

Complex contagion processes are commonly studied using *threshold models* (2, 11) where an individual adopts a behavior if the fraction of immediate connections engaging in the behavior exceeds a personal threshold. Granovetter (2) first proposes a threshold model to analyze the dynamics of collective human behaviors. The work by Granovetter (2) considers the problem of determining the number of people taking each action (e.g., the number of people adopting/not adopting the contagion) when the dynamics converges. He also investigates the stability of the convergence after perturbations of the initial threshold distribution. Since its introduction by Granovetter, variations of the threshold model on networks have been proposed and studied across numerous domains. Watts in his classic work (6) proposes a simply yet powerful model to examine the cascades of contagions on random networks. In Watts' model (6), individuals update their states based on the threshold rule, where the heterogeneous thresholds are selected from a distribution. Further, state updates happen in a random asynchronous order, and individuals' adoptions of the contagion are permanent throughout the dynamics (i.e., once an individual adopts the contagion, he/she continues to adopt it over the succeeding time steps). Based on the proposed model (6), Watts explores the correlations between the connectivity of a network and *rare* but *large* global cascades that are triggered by only small sets of initially active vertices. Watts shows that when the network is sparse, the cascade is modulated mainly by the overall connectivity of the network, where high-degree vertices are key triggers. In contrast, if the network is sufficiently dense, then the cascade is modulated by the local connectivity of individuals, where vertices with degrees around the average are key triggers. Our social contagion model can be seen as an extension of Watts' model (6), with the following key distinctions: $(i)$ Watts' dynamics is irreversible, that is, once an individual contracts the contagion (e.g., wears a mask), the adoption is permanent throughout the entire dynamics. In contrast, the mask-wearing states of individuals are *reversible* under our model, such that a person chooses **not** to wear a mask at a time step if none of the three conditions are satisfied. $(ii)$ individuals update states in random asynchronous order under Watts' model, whereas our model considers a synchronous update scheme. $(iii)$ our model further intertwines the social dynamics with the disease dynamics. We remark that the first distinction already implies a significant difference between the two models. For example, one primary cause of the observed critical transition in our model is the distinct time-series dynamics between the two regimes, shown in Fig 4 of the main manuscript. Note that, however, the oscillating dynamics of infection and mask adoption (i.e., Fig 4 $(a)$ and $(c)$) will not be observed if the mask-adoption is not reversible.

In another work by Dodds and Watts (12, 13), they propose a diffusion scheme that incorporates the mechanisms of independent cascade models (i.e., independent interaction models as stated in (13)) and threshold models. In particular, an individual $v$ has a state in $\{\mathtt{S}, \mathtt{I}, \mathtt{R}\}$ (or $\{\mathtt{S}, \mathtt{I}\}$ which depends on the model set up), and for each contact with another infected individual, $v$ receives a "dose" with some probability $p$. Each individual $v$ then maintains a *memory* of the accumulated doses over the past $T$ contacts, and $v$ contrasts the contagion if *the accumulated doses exceed a personal threshold*. They identify three classes of the dynamics (i.e., epidemic threshold, vanishing critical mass, and critical mass) and investigate transitions between the classes (13). Watts and Dodds (14) later studied the opinion formation processes by modeling the cascade of influence using a threshold scheme. They find that global cascades are often triggered by the group of people who can be easily influenced (i.e., their threshold values are relatively low), rather than the influential ones (14). Further, they consider various roles (e.g., initiators, early adopters) of people with different influential levels (e.g., influencals, hyperinfluentials) and investigate the

corresponding effects on global cascades.

Ramazi et al. (15) use the threshold model to study the agent decision-making processes in coordination/anti-coordination games. Note that when agents are anti-coordinating, a vertex $v$ becomes active if the fraction of *inactive* neighbors is at least a personal threshold of $v$. Ramazi et al. (15) show that under the asynchronous dynamics, the system almost always converges to an equilibrium in finite time, irrespective to the underlying network topology. Kuhlman et al. (16) introduce a "bi-threshold" model to study contagions (e.g., smoking behavior) where the adoption and the abandonment of the contagion requires different threshold. In particular, each individual $v$ has two thresholds $\tau_{up}$ and $\tau_{down}$, where $v$ becomes active when at least $\tau_{up}$ neighbors are active, and $v$ becomes inactive when at least $\tau_{down}$ neighbors are inactive. Kuhlman et al. (16) explore the complexity of different problems (e.g., convergence) in this model and preformced simulation on real-world datasets. Huang et al. (17) propose a variation of the threshold model that account for the effect of "persuasion". Each individual in this model (17) has two thresholds where the first threshold $\tau_1$ is the adoption threshold (i.e., an individual becomes active if the fraction of active neighbors is at least $\tau_1$), and the second threshold $\tau_2$ is the "persuasion threshold". In particular, a vertex becomes a persuader if the fraction of active neighbors is at least $\tau_2$, and a persuader can always successfully transmit the contagion to its neighbors (17). They show that the network becomes less robust under the influence of persuaders. The threshold model have also been studied in numerous contexts including evolution of discrete dynamical systems (18), networked games (19), disaster management (20), diffusion of innovations (21) and marketing (22).

**Multi-contagion models.** Many existing methods model the concurrent spread of social and biological contagions. Fu et al. (23) study the coupling of vaccination behaviors and the H1N1 flu epidemic in multiplex networks. In their model, an individual is in one of the following states {`S`, `I`, `R`, `V`} with some probability at each time step. The model is then a Markov chain over state space of $4^n$ state. They found that the vaccination decisions are affected by the vaccination states of neighbors as well as the prevalence of the disease (23). We stretch differences between Fu's model and our proposed model. First, the social and biological states are mutually exclusive in Fu et al., whereas in our proposed model, an individual simultaneously has a social state and a biological state. At the same time, the role of peer pressure in making vaccination decisions for a vertex is probabilistic, with a positive correlation to the number of vaccinated neighbors. In contrast, our model considers the threshold behaviors in obeying social norms. Moreover, fear is modeled probabilistically in Fu et al. (23) such that more infected neighbors yield a higher probability of taking vaccines. Note that such a generalization assumes the same fear threshold for all vertex. In our model, however, we give the option to individualize each vertex with a different threshold of fear and peer pressure. Lastly, Fu et al. (23) do not consider factors such as prosociality in triggering people to take vaccines (23).

Salathé and Bonhoeffer (24) also study the impact of vaccine opinions on the disease outbreak. Specifically, each vertex is assigned an initial opinion about vaccination, either negative or positive. The opinion dynamic is a probabilistic process (happens after opinion initialization) such that a vertex $v$ changes its opinion under a probability that is positively correlated to $v$'s neighbors with opposite opinions. After the opinion formation, people with positive opinions are vaccinated and become immune to the disease. The disease dynamic happens after vaccination which is again a probabilistic process specified by a transmission rate (24). Campbell and Salathé (25) study the spread of health behaviors and disease over the same network. Their model consists of two periods for which social and biological contagions spread in different periods, that is, their dynamics are not concurrent. In adopting the social behavior (refusal to take vaccines), they consider a threshold model based on the number of exposures to the neighbors who have adopted the social behavior. They also account for the exposures from other sources such as the media (25). Note that other factors such as prosociality or fear are not considered. After the social dynamic reaches a fixed point, the second period begins for which the disease spreads under the `SIR` disease model. Their results suggest that under the interplay of the social and disease dynamics, the structure of the underlying social network has a strong influence over outbreak size. In particular, they find that the outbreak size is maximized under small-world networks (25).

Funk et al. (26) investigate how responsive behaviors to an ongoing epidemic can influence the disease dynamic. In particular, they model the spread of awareness of the disease among the population by considering the number of hops the epidemic-related information has traveled before reaching an individual. The information that undergoes more passages then has a lower discounting factor on the transmissibility of the disease (26). Granell et al. (27) consider a microscopic Markov chain approach to model the interrelation between social and biological dynamics over multiplex networks. In particular, an individual becomes aware of the disease (which then takes countermeasures) either by contacting awarded neighbors or getting infected by the disease. Moreover, awareness can be forgotten with some probability. Lastly, the infectivity of disease-aware individuals gets discounted because of the health behaviors which they have adopted. In another work by Funk et al. (28) on modeling the spread of awareness and diseases, they use the `SIS` model for the social dynamic and the `SIRS` model for the disease dynamic. To incorporate the interplay between the two contagions, the infection rate gets discounted for those with disease awareness. An aligned work was conducted by Hébert-Dufresne (29) who also consider the concurrent spread of awareness and disease on highly clustered networks. In particular, the social dynamics of awareness dampens the infection rate, and the disease dynamics increases the transmission rate of awareness. They make an interesting case where an increase in the clustering of networks could incur larger epidemics.

Epstein et al. (30) model the interacting dynamics of fear and the disease. In their method, an individual contracts fear with a fixed per-contact probability from neighbors who are infected or who are afraid of the disease (or both). In response to fear, people are removed from the circulation, and those who have been removed are put back into circulation at some given rate. Overall, they observe multiple waves of infections under the proposed dynamics. Gross et al (31) tackle the problem from another perspective for which a susceptible can take countermeasures by breaking a link to an infected neighbor and rewiring to some other susceptible under a given probability. Their result shows that under the adaptive rewiring, the network could be updated to two clusters of susceptible and infected, respectively. Cencetti and Battiston (32) study a multiplex network model where contagions can disseminate across different layers. They show that when the two layers and drastically different, the rate of the diffusion process is maximized when the cross-layer interaction is high. They also suggest that the diffusion rate is determined by the layer with the least velocity. Alvarez-Zuzek et al. (33) also investigate the co-evolution of the opinion about vaccination (as a social contagion) and a disease over multiplex networks. In particular, they simulate the diffusion of the opinion about vaccination using the M-model, which consists of two concurrent processes: persuasion and compromise. On the other hand, the disease model is the `SIRV` model under the effectiveness of vaccination. They find that as the vaccine gets more effective, the number of recovered individuals decreases since fewer infections occur. They also suggest a threshold value of the vaccine effectiveness, such that the epidemic will not persist if the vaccine effectiveness is above the threshold. In contrast, the epidemic will always develop despite the vaccine effectiveness when the transmission probability is high enough (33). Jovanovski et al. (34) study the multi-contagion `SIS` model over multiplex networks. They analyze the bounds of the basic reproduction number of the proposed dynamic and characterize the dependence of the epidemic threshold to the network structure.

Many existing models study the interplay between human behaviors and diseases from economic perspectives. Toxvaerd (35) proposes a framework where individuals can perform social distancing under a non-cooperative decision-making pattern. Toxvaerd shows that the social dynamic reaches an equilibrium when the disease prevalence is at its highest. Another work by Toxvaerd (36) considers a model under a decentralized decision pattern where individuals can overexpose to disease. The results show a negative correlation between induced infection risks increases and prevalence, subsequently, a high disease prevalence leads to a drop in the overall welfare. David et al. (37) extend the SEIR model to explore how testing and quarantine impact the disease dynamic. In particular, they establish that a large range of testing under targeted quarantine can effectively lessen the negative influence on the economy. There is a plethora of other models that investigate the dueling dynamics and economic impacts (38–40).

**Behavioral responses.** We give a short overview of the literature supporting the factors that in our model triggers individuals' mask-wearing behaviors: *peer pressure*, *fear for infection*, and *prosociality*.

**Peer pressure.** Extensive literature supports that behaviors are shaped by social norms (41, 42). Particularly, research has shown that peer pressure plays an important role in people's mask-wearing decisions. For instance, Bokemper et al. (43) conducted a study via online survey over U.S and Italy to understand the role of peer influence in mask-wearing. Their results show that more people wearing masks enforce the social norm, leading to more compliance among the population. Moreover, people sometimes judge those who do not wear masks which further increases the social pressure (43). Another study by Hansstein and Echegaray (44) shows that college students wear masks because it is "socially appropriate" to do so. In particular, their adaption of this prosocial behavior is greatly influenced by friends and roommates. Similar results were given by Barcelo and Sheen (45) which suggests that people are more likely to wear masks if they live in a region where mask-wearing is common. Lastly, DeJonckheere et al. (46) conducted a survey for $1,087$ youth. They considered different factors in mask-wearing. In particular, they show that 15.7% of the participants wear masks because of peer pressure.

Social conformity can be captured by **threshold models**. In the classic work by Granovetter, a simple model is considered where each people have a threshold of peer influences, and they decide to take action if the number of peers who take actions exceeds the threshold (2). In another study, Wolf et al. (47) conducted social experiments on college students in Germany to understand their decision-making process. They found that students use quorum thresholds as a strategy, and this threshold is set based on the decisions made by people around them.

**Fear for infection.** Fear is an adaptive human response to unprecedented diseases like COVID-19 (48). The fear for COVID-19 is triggered by different sources, including the media coverage of the number of confirmed cases and the death toll. Bendau et al conduct a survey on $6,233$ participants in Germany, where they find a positive correlation between COVID-related media consumption and anxiety and depression. Furthermore, those with pre-existing fear for health conditions are more likely to spend time watching the news which leads to a higher level of fear (49). Similar results are suggested by Mertens et al. (50) where they give online surveys to 439 participants, and found that media usage is associated with an increased level of fear. Other factors that cause fear include the health of others, personal health, Food shortage, etc. Liu et al. (51) study the social enforcement process over multiplex networks. They identify the co-existence of extinction and outbreak states both analytically and experimentally. More reverent to our work, Liu et al. (51) also show the existence of a critical transition for the bi-stability. Fitzpatrick et al. (52) conduct online surveys on over $10,368$ individuals in U.S. Overall, they find that the general population is fearful for COVID. In particular, they suggest that the level of fear is higher and more concentrated in urban areas and areas with high numbers of cases, that is, the fear is not equally distributed. Also, certain demographics such as female, Asian, Hispanic, etc have a higher level of fear (52). Different scales are designed to evaluate the level of fear experienced by individuals. In particular, Ahorsu et al. (48) introduce a seven-item scale where they show a high correlation between fear of COVID and depression.

People put on face masks in response to the fear for COVID-19. Huynh (53) conducted a survey on 345 individuals in Vietnam and the results suggest a positive correlation between the fear for COVID-19 and the likelihood of wearing masks. It is also shown that wearing masks can reduce the fear of infection and encourage people to participate in daily activities (54). Nakayachi et al. (55) surveyed $1,000$ participants to examine the factors that incentivized mask adoption. Apart from a strong correlation between peer influence and mask usage, feeling relief from fear and anxiety is the second most prominent factor that triggers mask-wearing (55).

**Prosociality.** Prosocial behaviors are defined as actions with motivations for promoting human welfare. Research has shown that prosocial individuals exist in many societies (56–58). In this work, we assume that prosocial people put on masks voluntarily.

## Methodology in Selecting Baseline Parameters

This section presents the methodology in choosing the baseline values for social and disease parameters shown in Table (S2). In general, we assume that a fraction of the population is of the prosocial type. Further, We allow fear and peer pressure thresholds of individuals to be heterogeneous. Specifically, the peer pressure/fear threshold of each individual is assigned uniformly at random from a range.

**The fraction of the prosocial population.** Given that the U.S. has no mask-wearing habit, we assume that no individuals wear masks on the first day of the epidemic. To model society with a low prosociality level, we set 1% of the population to be *prosocial individuals* who wear masks voluntarily during the epidemic period. In our numerical experiments, we vary the population's prosocial level to characterize different societies.

**The range of fear threshold.** As shown in the related work section, extensive research stretches the critical role of fear in the dueling of social and disease dynamics. However, to the best of our knowledge, they do not provide information regarding the *thresholds of fear* considered in our model. To get insight for a lower bound of fear threshold, we attempted to refer to the number of infections in the U.S. at the time (Mar 13, 2020) when the White House declared the national emergency[†]. However, the corresponding number[‡] is only $1,268$, which is statistically negligible compared to the U.S. population. Nevertheless, we set the lower bound of fear to 0.001, a value that accounts for the minuscule fraction of infection referred above, yet, still statistically significant. As for an *upper bound for fear*, at the time of writing, the number of reported cases of COVID in the U.S. is $36,118,278$, which is roughly 10% of the entire population, and this number is enough to trigger a very high adoption rate of mask-wearing (under other measures such as government mandates). Thus, we set the upper bound of fear to 0.15 to account for the stubborn people who are inflexible in adopting masks.

**The range of peer pressure threshold.** In social science studies, Wolf et al. (47) suggest that the peer influence thresholds could range from 0.1 to 0.8. Moreover, He et al. (59) and Kahane (60) found that there always exists stubborn people who are unlikely to wear masks. Overall, we set the lower and the upper bound of the peer pressure to 0.3 and 1.0, respectively. Specifically, the lower bound 0.3 accounts for those easily influenced by peers, and the upper bound 1.0 accounts for the stubborn individuals.

**Discounting factor for masks.** There are plenty of existing studies on the *effectiveness of masks* in preventing disease spread. Brienen et al.(61) show that the infectious risk after wearing masks decreases almost linearly w.r.t. the mask effectiveness. Leung et al. (62) conducted studies on mask-wearing as a mitigation strategy for COVID and flu. They screened $3,363$ individuals. For the group without face masks, up to 30% and 36% of the participants were infected by COVID and influenza virus, respectively. On the other hand, the infection rates for the group with masks are reduced to 0% and 4%. Eikenberry et al. (63) estimate the inward mask efficiency to be up to 80% for cloth masks, 70% to 90% for surgical masks, and over 95% for N95's. Patel et al. suggest a similar result where 80% to 90% of particles released from the infectious source can be captured by masks (64). All the results suggest the high effectiveness of masks. As for the differences between sources and receiver efficacy, Diza et al. (65) show that wearing masks at the source is at least 3 times more effective than wearing masks at the receiver. Overall, we set the receiver discounting factor $\alpha = 0.3$ and the source discounting factor $\beta = 0.1$ to capture $(i)$ the high effectiveness of masks, and $(ii)$ the difference between masks on sources and receivers. Lastly, following epidemiological literature, we set the expected *infectious period* to 9 days ($r = 1/9$) (66, 67).

Despite the explicitness of the baseline parameter values, we employ various parameter settings in experiments to account for diverse testing scenarios. In particular, the critical transition of dueling dynamics is observed under different ranges of fear and peer pressure thresholds, different percentages of prosocial people in society, and different mask effectiveness.

[†] www.ajmc.com/view/a-timeline-of-covid19-developments-in-2020

[‡] (www.statista.com/statistics/1103185/cumulative-coronavirus-covid19-cases-number-us-by-day/)

**Table S2. Baseline parameters**

| Parameter | Description | Baseline value | Ref. |
|---|---|---|---|
| $p_s$ | Fraction of prosocial population | $0.01$ | Assumed |
| $p_i$ | Fraction of population wearing masks on day $1$ | $0.00$ | Assumed |
| $l_f$ | A lower bound of the threshold for fear | $0.001$ | Assumed |
| $u_f$ | An upper bound of the threshold for fear | $0.15$ | Assumed |
| $l_p$ | A lower bound of the threshold for peer pressure | $0.3$ | (47, 68) |
| $u_p$ | An upper bound of the threshold for peer pressure | $1.0$ | (59, 60, 69) |
| $\alpha$ | Discounting factor for a susceptible individual wearing a mask | $0.3$ | (62–64, 70) |
| $\beta$ | Discounting factor for an infected wearing a mask | $0.1$ | (62–64, 70) |
| $r$ | Recovery rate | $1/9$ | (67) |

## Oscillations of Infection and Masks Usage in the State of Virginia

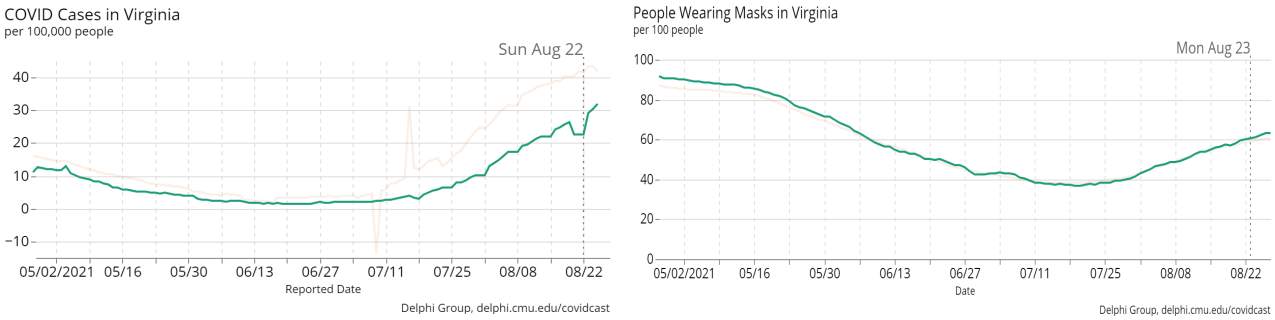


**(a)** Covid Cases in Virginia

**(b)** The number of people wearing masks in Virginia

**Fig. S1.** The number of Covid cases and the number of people wearing masks in Virginia from $05/02/2021$ to $08/22/2021$. The plot is generated by `COVIDCast`. Overall, we observe an oscillation of infection and mask adoption.

## Robustness of the critical transition

In this section, we demonstrate the robustness of the critical transition. Specifically, we study its persistence under various parameter settings, network structures, and model extensions.

***Robustness with respect to model parameters.*** We explore the influence of social and disease parameters on the critical transitions of the joint dynamics. In particular, we consider variations of $(i)$ percentage of prosocial individuals in a society, $(ii)$ ranges of peer pressure thresholds, $(iii)$ ranges of fear thresholds, $(iv)$ mask effectiveness, $(v)$ network density, and $(vi)$ initialization of only high/low degree nodes to be infected.

Figure S2 depicts the coupling of social and disease dynamics in four societies with different percentages of prosocial individuals: 0.01, 0.1, 0.2, 0.3, respectively. Overall, the system exhibits a critical transition under various prosocial percentages. Furthermore, the critical transition is more prominent in society with a low fraction of prosocial individuals. Specifically, the critical transition diminishes under a society with 30% of the prosocial population. This correlation is expected since the critical transition is driven by the level of mask usage among the population.

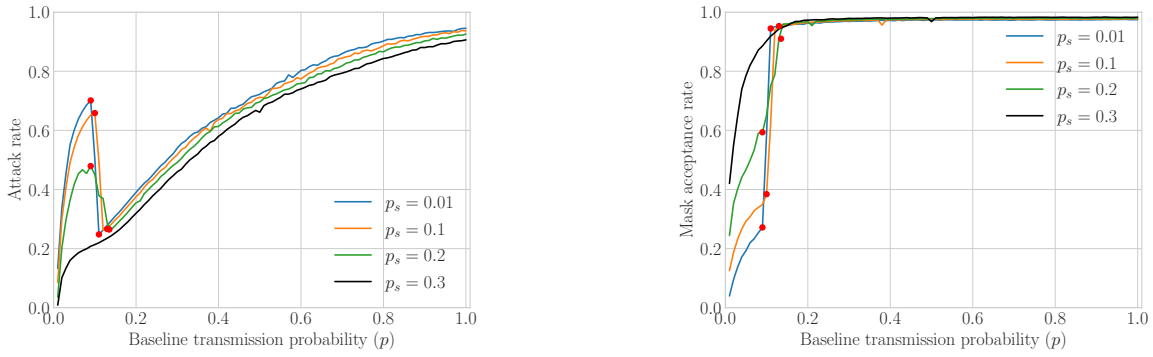


**(a)** Attack rate as a function of $p$

**(b)** Mask acceptance rate as a function of $p$

**Fig. S2. Dueling dynamics under different prosocial percentages $p_s$.** We consider four societies with various *percentages of prosocial individuals*: $p_s = 0.01, 0.1, 0.2, 0.3$, respectively. Panel $(a)$ depicts the attack rate as a function of the baseline transmission probability $p$. Panel $(b)$ plots the mask acceptance rate as a function of $p$. All other parameters are set to their baseline values shown in Table S2. Overall, the critical transition persists before $p_s$ reaching $0.3$. We also observe a diminishing magnitude of critical transition as the fraction of prosocial individuals increases.

Results on the effect of other parameters are shown in Figure S3 to Fig S8. Here, we summarize the main findings. **The critical transition of the dueling dynamics are observed under a broad spectrum of model parameters.** In particular, the critical transition is more pronounced when $(i)$ there are fewer prosocial people in the

society; (*ii*) people are more fearful of the disease; (*iii*) people are less sensitive to peer pressure; (*iv*) masks are more effective. Moreover, the critical transition persists irrespective of the connectivity of initially infected individuals (i.e., degrees).

We also conducted an *ablation study* to determine if the critical transition is a combined effect of both *peer pressure* and *fear*. Specifically, we remove one component (i.e., p*eer pressure* or *fear*) from the network model and explore the attack rate as a function of baseline transmission probability. The result is shown in Fig S9. Overall, the dueling dynamics do not undergo critical transitions in the absence of fear or peer pressure, suggesting the necessity of both components.

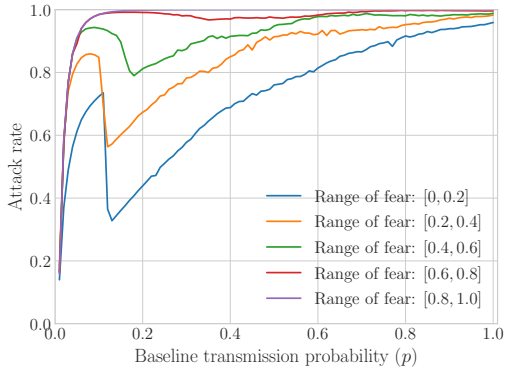


**(a)** Attack rate as a function of $p$

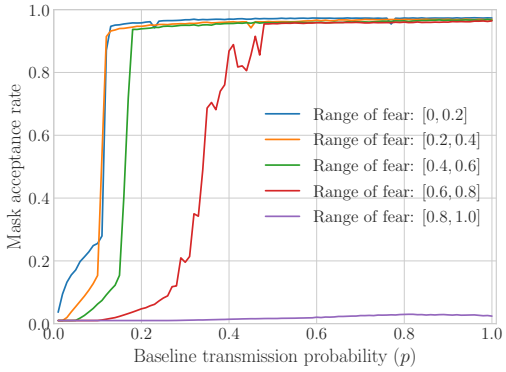


**(b)** Mask acceptance rate as a function of $p$

**Fig. S3. Dueling dynamics under different levels of fear.** We consider varying ranges of *fear* thresholds in the population: $[0, 0.2]$, $[0.2, 0.4]$, $[0.4, 0.6]$, $[0.6, 0.8]$, $[0.8, 1.0]$. In particular, the fear threshold for each individual is chosen uniformly at random within a specified range. Panel $(a)$ shows the attack rate as a function of the baseline transmission probability $p$. Panel $(b)$ plots the mask acceptance rate as a function of $p$. All otehr parameters are set to their baseline values shown in Table S2. Overall, we observe that the critical transition is more pronounced when people are more fearful of the disease.

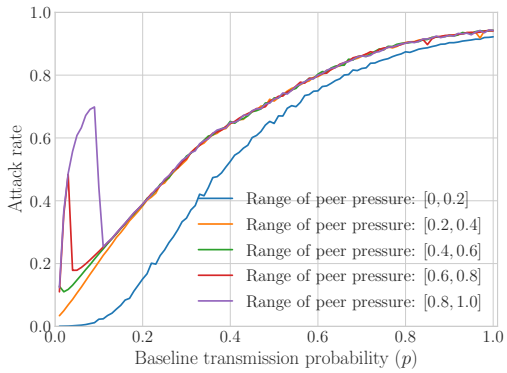


**(a)** Attack rate as a function of $p$

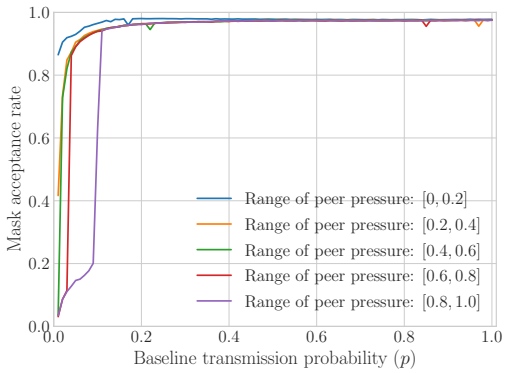


**(b)** Mask acceptance rate as a function of $p$

**Fig. S4. Dueling dynamics under different levels of peer pressure.** We consider varying ranges of *peer pressure* in the population: $[0, 0.2]$, $[0.2, 0.4]$, $[0.4, 0.6]$, $[0.6, 0.8]$, $[0.8, 1.0]$. In particular, the peer pressure threshold for each individual is chosen uniformly at random within a specified range. Panel $(a)$ shows the attack rate as a function of the baseline transmission probability $p$. Panel $(b)$ plots the mask acceptance rate as a function of $p$. All other parameters are set to their baseline values shown in Table S2. Overall, the critical transition is more pronounced when people are less sensitive to the peer pressure.

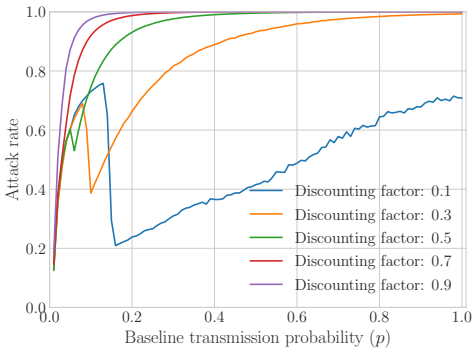


**(a)** Attack rate as a function of $p$

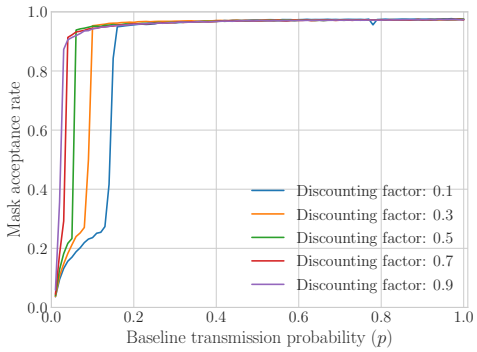


**(b)** Mask acceptance rate as a function of $p$

**Fig. S5. Dueling dynamics under different mask effectiveness.** We consider masks with different discounting factors ($\alpha$ and $\beta$ are set to be the same) from $0.1$ to $0.9$. Panel $(a)$ shows the attack rate as a function of the baseline transmission probability $p$. Panel $(b)$ plots the mask acceptance rate as a function of $p$. All other parameters are set to their baseline values shown in Table S2. Overall, the critical transition is more pronounced when masks are more effective.

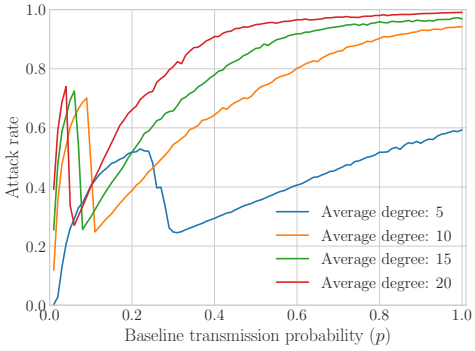


**(a)** Attack rate as a function of $p$

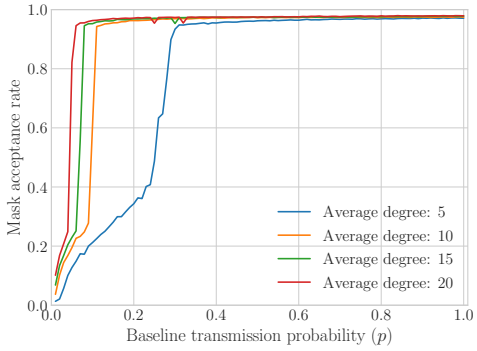


**(b)** Mask acceptance rate as a function of $p$

**Fig. S6. Dueling dynamics under various averaged degrees.** We vary the averaged degrees of the two-layer networks from $5$ to $20$. Panel $(a)$ shows the attack rate as a function of the baseline transmission probability $p$. Panel $(b)$ plots the mask acceptance rate as a function of $p$. All other parameters are set to their baseline values shown in Table S2. We observe that the critical transition is more pronounced when the network density increases.

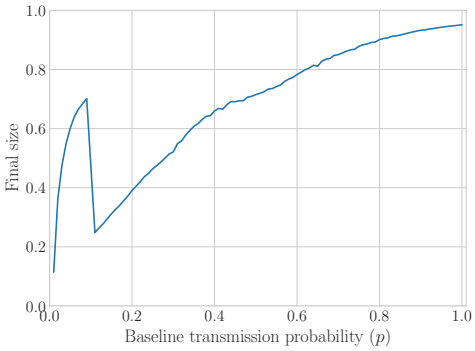


**(a)** Attack rate as a function of $p$

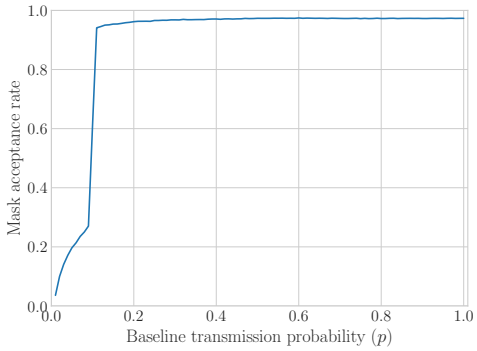


**(b)** Mask acceptance rate as a function of $p$

**Fig. S7. Dueling dynamics under initializations of high degree nodes.** The plot depicts the coupling of social and disease dynamic when the $10$ initially infected nodes are randomly chosen from the top $20\%$ of the population with the **highest** degrees. Panel $(a)$ shows the attack rate as a function of the baseline transmission probability $p$. Panel $(b)$ plots the mask acceptance rate as a function of $p$. All parameters are set to their baseline values shown in Table S2. We observe that the critical transition persists under this setting.

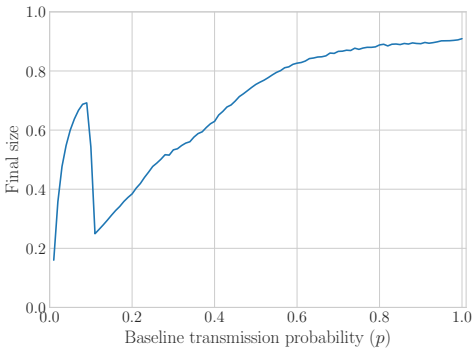


**(a)** Attack rate as a function of $p$

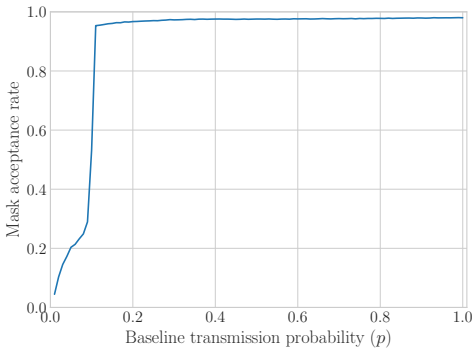


**(b)** Mask acceptance rate as a function of $p$

**Fig. S8. Dueling dynamics under initializations of low degree nodes.** The coupling of social and disease dynamic when the 10 initially infected nodes are randomly chosen from the top 20% of the population with the **lowest** degrees. Panel $(a)$ shows the attack rate as a function of the baseline transmission probability $p$. Panel $(b)$ plots the mask acceptance rate as a function of $p$. All parameters are set to their baseline values shown in Table S2. Similar to the setting in Fig S7, we also observe a critical transition when low degree nodes are initially infected.

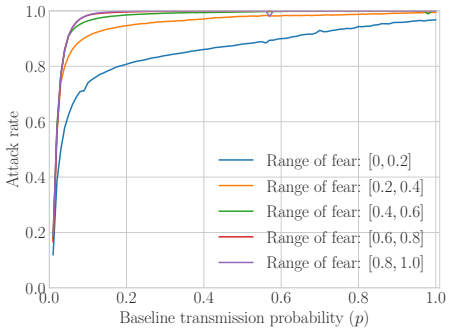


**(a)** Attack rate as a function of $p$ in the absence of peer pressure.

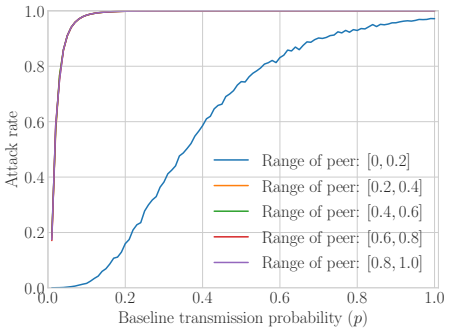


**(b)** Attack rate as a function of $p$ in the absence of fear.

**Fig. S9. Ablation study of the dueling dynamics.** We investigate if the critical transition is a joint effect of fear and peer pressure. The figure shows the attack rate as functions of the transmission probability with either fear or peer pressure component removed from the model. In particular, panel $(a)$ depicts the disease dynamic in the absence of peer pressure, under different levels of fear in the population. Panel $(b)$ shows the disease dynamic in the absence of fear fraction, under different levels of peer pressure in the population. All other parameters are set to their baseline values shown in Table S2. Overall, the dynamics do not undergo critical transitions in the absence of fear or peer pressure, suggesting the necessity of both components.

***Robustness with respected to network structures.*** We conducted experiments on two classes of networks: $(i)$ power-law networks with a small number of high degree nodes, and $(ii)$ Erdös–Rényi networks where most vertices have similar degrees. Specifically, we simulate the dueling dynamics on power-law networks of sizes up to $100,000$ with exponents $\gamma$ from 2.35 to 3.39. Overall, the critical transition occurs in all the tested networks. Fig S10 $(b)$ illustrates the critical transition under power-law networks of size $100,000$ with varying $\gamma$. Overall, we observe the corresponding attack rate at the first tipping point increases as $\gamma$ increases.

Fig S10 $(a)$ shows the the disease dynamic for Erdös–Rényi graphs of size $100,000$ with varying average degrees $\bar{d}$ from 1 to 9. In particular, we observe an emergence of the critical transition as the average degree increases. This occurs partly due to the increased the social dynamic strength as the network gets well connected. We further explored Erdös–Rényi networks with higher average degrees, and the critical transition persisted. We also remark that the critical transition exists even when the two network layers are drastically different. That is, each layer is a newly generated random network of the same class (instead of undergoing edge perturbations over the same baseline network).

Overall, our numerical explorations suggest that the emergence of the critical transition is mainly driven by

the coupling between the behavioral response model and the epidemic dynamics. While some effects on the joint dynamics are observed, the critical transition is shown to be robust to varying characteristics of the underlying network structures.

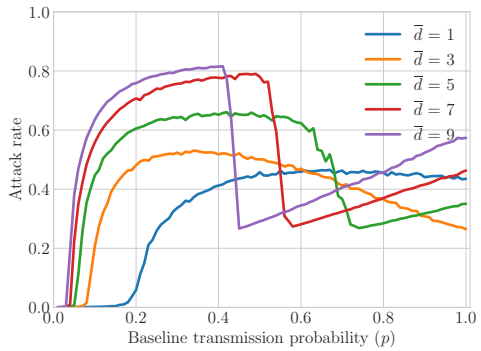


**(a)** The robustness of the critical transition under gnp networks

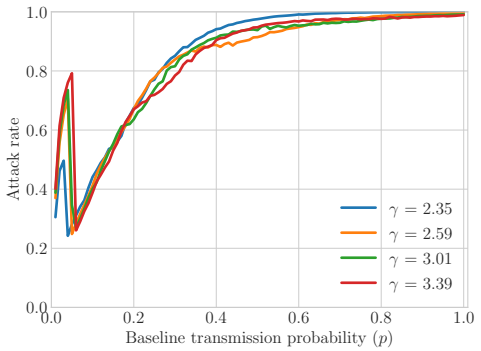


**(b)** The robustness of the critical transition under power-law networks

**Fig. S10. The robustness of the critical transition under different network structures**. The figure depicts the baseline transmission probability as a function of attack rate, under power-law and gnp network, respectively. Panel $(a)$ shows the results on gnp networks networks of size $100,000$, with average degree $\bar{d}$ from $1$ to $9$. Panel $(b)$ depicts the results on power-law networks of size $100,000$ with exponents $\gamma$ from $2.35$ to $3.39$. All parameters are set to their baseline values shown in Table S2.

**Results for Model extensions.** We study the persistence of the critical transition under two extensions of the behavior model. In the first extension, we incorporate the *habit formation process* into the mask-wearing dynamics. Specifically, each individual $v$ is associated with $\epsilon_v \in [0,1]$, denoting the strength of the mask-wearing habit. If $v$ chooses to wear a mask (either due to fear or peer pressure) on any given day, he or she continues to wear a mask the next day with probability $\epsilon_v$. Conversely, if $v$ takes off the mask, the social dynamic switches back to the threshold-based model. The result is shown in Fig S11. Overall, we observe critical transitions of the disease dynamic under various habit strengths of the population. In particular, the critical transition exhibits a negative correlation to the habit strength, such that the lower the strength, the sharper the critical transition.

In the second extension, we introduce the asymptomatic state to the model. In particular, a fraction of the infected population is *asymptomatic*, and only *symptomatic* infections can trigger fear in the population. The results are shown under Fig S12 and Fig S13, where we investigate the dueling dynamics under different ratios of symptomatic to asymptomatic infections. Overall, the critical transition persists under a broad range of symptomatic to asymptomatic ratios.

***Habit formation.*** Let $\epsilon_v \in [0,1] : v \in V$ be the *strength* of the mask-wearing habit for an individual $v$ such that if $v$ chooses to wear a mask (due to fear or peer pressure) on a given day, then with probability $\epsilon_v$, he continuous to wear a mask in the next day due to the habit. Let $a_4^{(t)}(v)$ be the indicator variable such that $v$ wears a mask at time $t$ due to the habit, then an individual wears a mask at time $t$ if $a_1 \vee a_2^{(t)}(v) \vee a_3^{(t)}(v) \vee a_4^{(t)}(v)$ is satisfied. If $v$ takes off the mask at any time, the social dynamic switches back to the threshold-based model. We remark that the original dueling model is a special case of this extend model under $\epsilon_v = 0, \forall v \in V$.

The result is shown in Fig S11. Overall, we observe critical transitions of the disease dynamic under various habit strengths. Specifically, the critical transition exhibits a negative correlation with the habit strength such that the lower the strength, the sharper the critical transition.

***Only symptomatic infections trigger fear.*** We consider an extension of the model where a fraction of the infected population is *asymptomatic*, and we only consider the total number of *symptomatic* infections in triggering fear. The results are shown under Figure S12 and Figure S13 where we investigate the dueling dynamics under different ratios of

symptomatic to asymptomatic infections. Overall, the critical transition persists under a broad range of symptomatic to asymptomatic ratios.

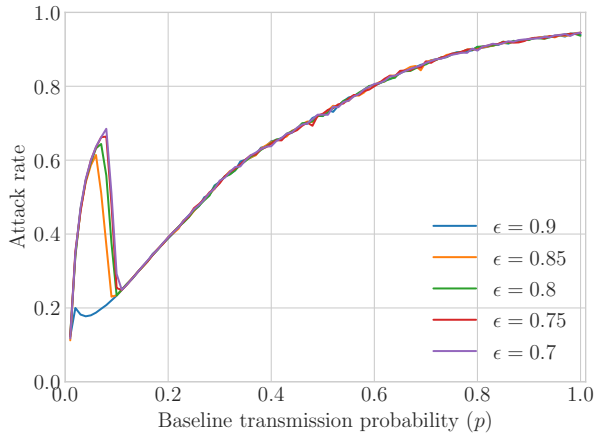


**Fig. S11. critical transition under different habit strengths** $\epsilon$ (the probability of continuing wearing a mask). The plot shows the transmission probability as a function of attack rate under different habit strengths from $0.9$ to $0.7$. All other parameters are set to their baseline values shown in Table S2.

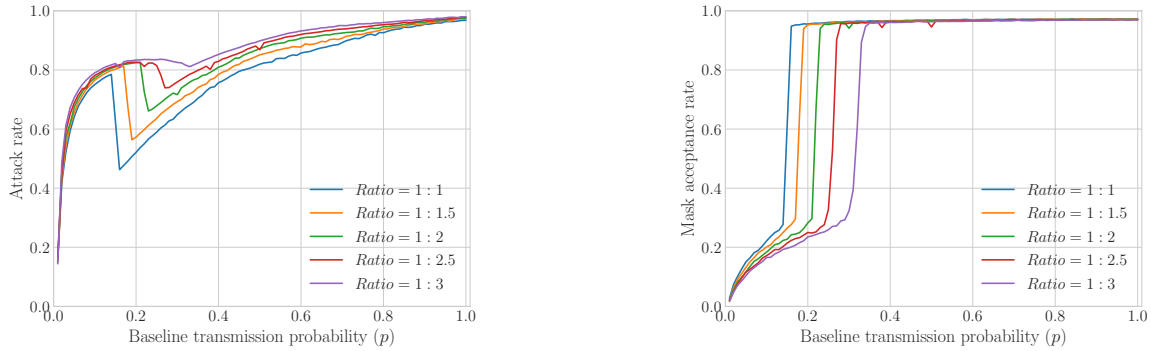


**(a)** attack rate as a function of $p$

**(b)** mask acceptance rate as a function of $p$

**Fig. S12. Dueling dynamics under different symptomatic to asymptomatic infections ratios.** We consider different ratios of **symptomatic to asymptomatic** infections where there are more asymptomatic cases. Panel $(a)$ shows the attack rate as a function of transmission probability $p$. Panel $(b)$ plots the mask acceptance rate as a function of transmission probability. All other parameters are set to their baseline values shown in Table S2.

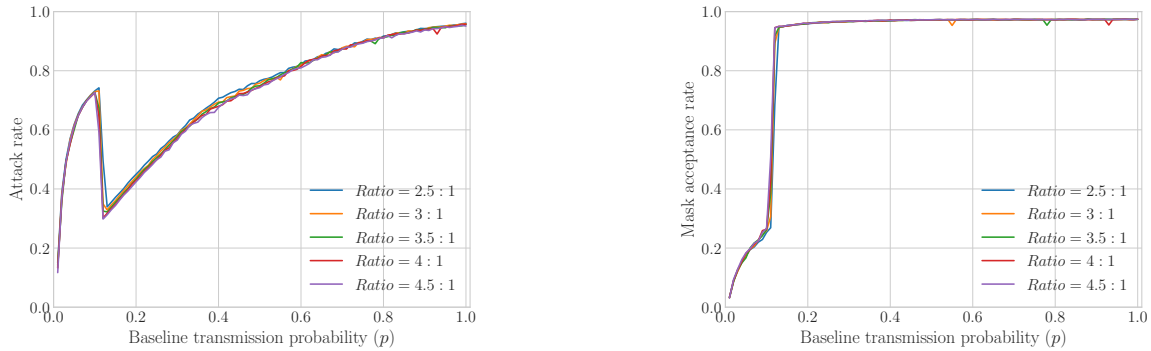


**(a)** attack rate as a function of $p$

**(b)** mask acceptance rate as a function of $p$

**Fig. S13. Dueling dynamics under different symptomatic to asymptomatic infections ratios.** We consider different ratios of **symptomatic to asymptomatic** infections where there are more symptomatic cases. Panel $(a)$ shows the attack rate as a function of transmission probability $p$. Panel $(b)$ plots the mask acceptance rate as a function of transmission probability. All other parameters are set to their baseline values shown in Table S2.

**Robustness on real-world networks.** Lastly, we investigate the robustness of the critical transition on a realistic social contact network. It is a digital twin of Manassas city, Virginia, social contact network. The network has about $35,000$ nodes and an average degree of 14. The digital twin is generated by (i) constructing synthetic individuals and locations; (ii) assigning daily activity sequences to each individual; (iii) mapping each activity of each individual to a location with the associated visiting time interval; (iv) deriving edges between people from their physical proximity when they visit the same location at the same time. The detailed steps of the construction of such a digital twin for any county or state level region in the U.S.A. are described in (71) and more details of the methodology can be found in (72–74). Here we consider the unweighted version of the Manassas network with the same parameter values in Table S2. The results are shown in Figure S14. Overall, the critical transition of the dueling dynamics persists in the Manassas social contact network. Note that the observed critical transition is less pronounced compared with other synthetic networks' results. Remark that the magnitude of a critical transition (i.e., absolute difference of values on the y-axis between the two tipping points) is affected by the parameter setting; thus, we can produce sharper critical transitions by varying the model parameters.

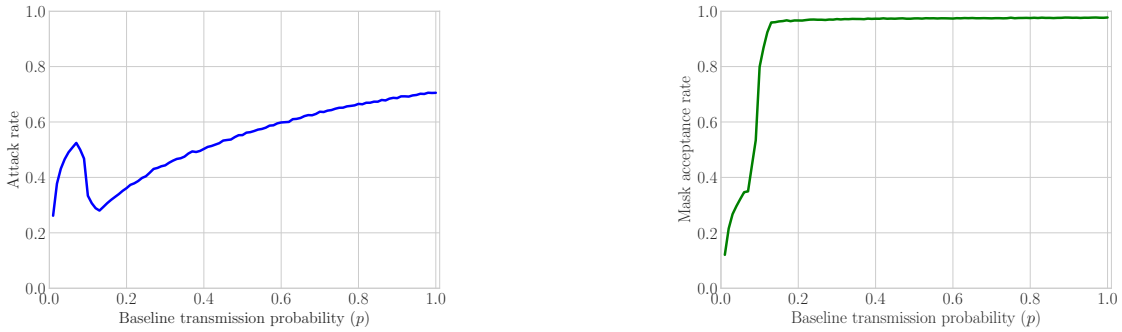


**(a)** attack rate as a function of $p$

**(b)** mask acceptance rate as a function of $p$

**Fig. S14. Dueling dynamics in Manassas networks.** The plot depicts the coupling of social and disease dynamic for the Manassas networks of size 35,028 with an average degree of $14$. Panel $(a)$ shows the attack rate as a function of transmission probability $p$. Panel $(b)$ plots the mask acceptance rate as a function of transmission probability. All parameters are set to their baseline values shown in Table S2. Overall, we observe a critical transition of the social and biological dynamics. Remark that the critical transition is sensitive to the parameter setting, as we can make it more pronounced by changing the model parameters.

## A different view of the time-series dynamics between the two regimes

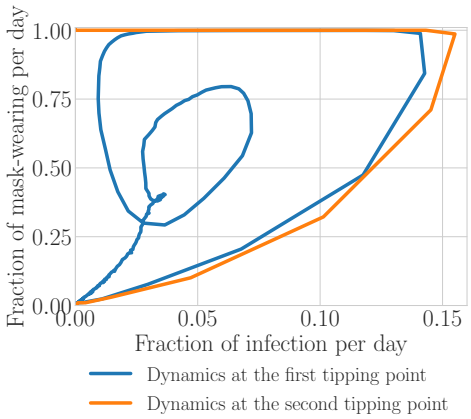


**Fig. S15. A different view of the time-series dynamics between the two regimes.** We depict the time-series dynamics of infection and mask adoption at the first and the second tipping point, respectively. See for further explanation and discussion using a compartmental model.

## Robustness of the causes of the critical transition

As show in the main manuscript, one cause of the critical transition is the distinct time-series dynamics of the two regimes. Specifically, the infection and mask adoption dynamics exhibits multiple waves when the disease baseline transmission probability $p$ is in the first regime. In contrast, infection and mask adoption dynamics undergoes only a single wave when $p$ is in the second regime. This section demonstrates the robustness of this underlying mechanism driving the critical transition. In particular, the study is performed under different parameter setting with variations on $(i)$ range of peer pressure thresholds; $(ii)$ range of fear thresholds, and $(iii)$ fraction of the prosocial population. Overall, when critical transitions appear, we observe the contrasting dynamics under all tested parameters. Example time-series dynamics are at the first/second tipping points of the critical transition, shown from Fig S16 to S18.

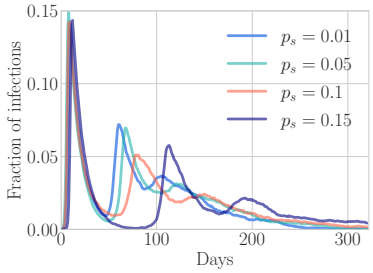


**(a)** Disease dynamics at the first tipping point

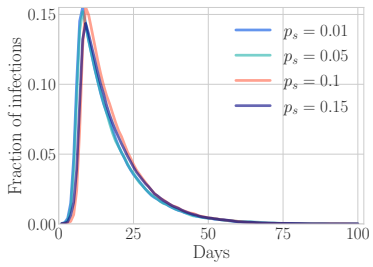


**(b)** Disease dynamics at the second tipping point

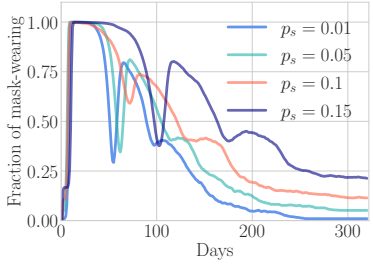


**(c)** Mask dynamics at the first tipping point

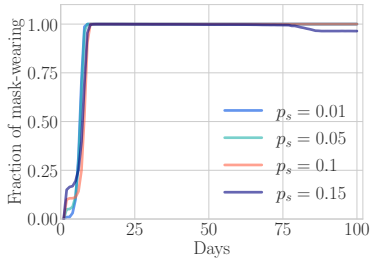


**(d)** Mask dynamics at the second tipping point

**Fig. S16. The time-series dynamics of disease and mask adoption at the tipping points under varying prosocial percentages** $p_s$. Panels $(a)$ and $(c)$ depict the time-series dynamics at the first tipping point. Panels $(b)$ and $(d)$ depict the time-series dynamics at the second tipping point. The percentage of prosocial population ranges from $0.01$ to $0.15$. The baseline transmission probability is fixed to the values at the tipping points. All other parameters are set to their baseline values shown in Table S2.

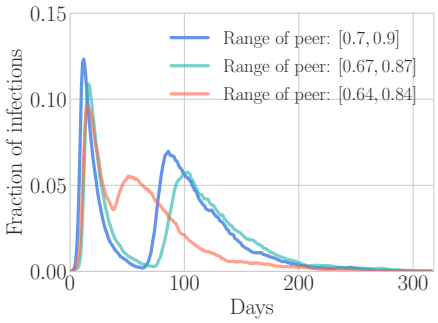


**(a)** Disease dynamics at the first tipping point

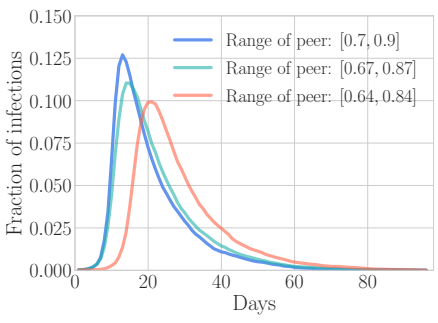


**(b)** Disease dynamics at the second tipping point

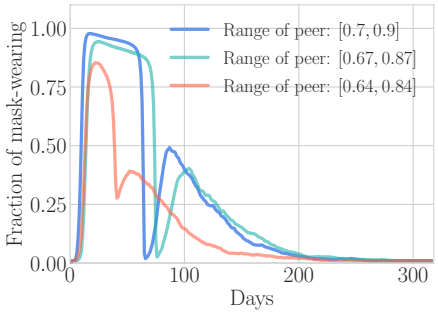


**(c)** Mask dynamics at the first tipping point

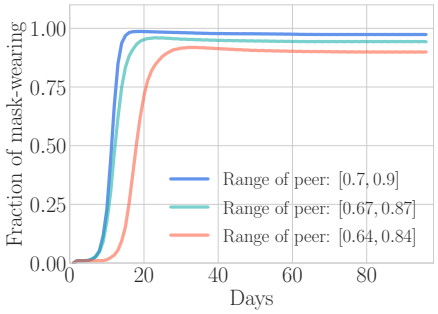


**(d)** Mask dynamics at the second tipping point

**Fig. S17. The time-series dynamics of disease and mask adoption at the tipping points under varying ranges of peer pressure thresholds**. Panels $(a)$ and $(c)$ depict the time-series dynamics at the first tipping point. Panels $(b)$ and $(d)$ depict the time-series dynamics at the second tipping point. The range of peer pressure threshold varies from $[0.7, 0.9]$ to $[0.64, 0.84]$. The baseline transmission probability is fixed to the values at the tipping points. All other parameters are set to their baseline values shown in Table S2.

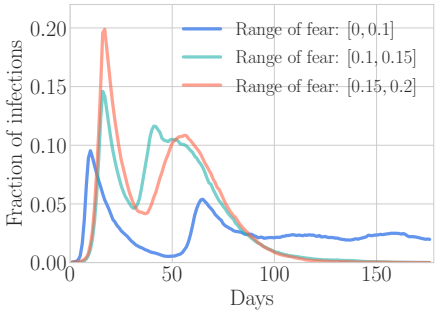


**(a)** Disease dynamics at the first tipping point

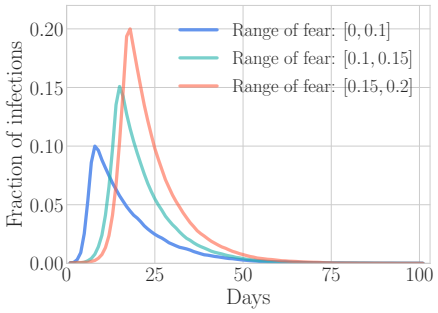


**(b)** Disease dynamics at the second tipping point

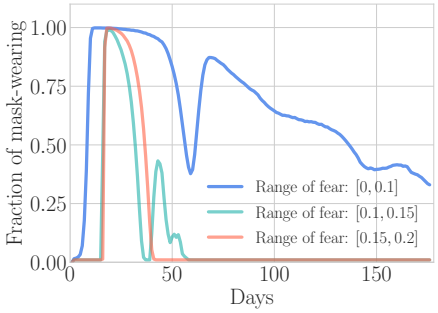


**(c)** Mask dynamics at the first tipping point

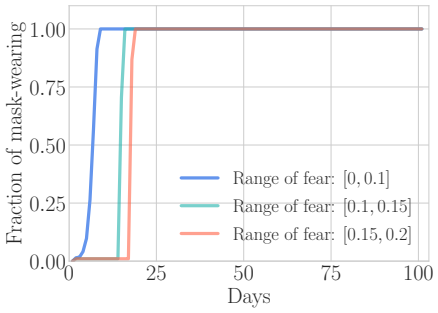


**(d)** Mask dynamics at the second tipping point

**Fig. S18. The time-series dynamics of disease and mask adoption at the tipping points under varying ranges of fear thresholds**. Panels $(a)$ and $(c)$ depict the time-series dynamics at the first tipping point. Panels $(b)$ and $(d)$ depict the time-series dynamics at the second tipping point. The range of fear threshold varies from $[0, 0.1]$ to $[0.15, 0.2]$. The baseline transmission probability is fixed to the values at the tipping points. All other parameters are set to their baseline values shown in Table S2.

## Enforcement of mask-wearing tames epidemic waves

We further explore the infection dynamic under public mask-wearing mandates. In particular, when the disease prevalence starts to lessen, we enforce mask-wearing individuals to continue wearing masks in spite of the reduction in peer pressure and fear. Subsequently, as shown in Figure S19, we can effectively suppress the disease revival and bring the anticipated oscillation of infection down to only a single wave. This observation highlights the importance of continuing mask mandate despite a low level of disease prevalence and social stigma.

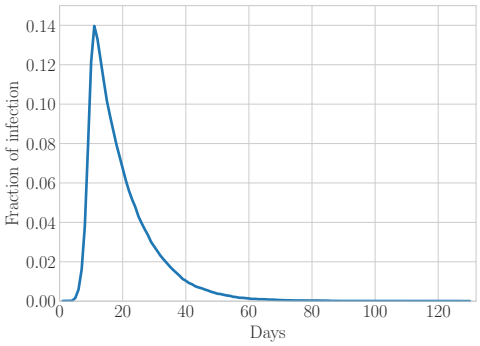


**(a)** Evolution of infection under the first tipping point

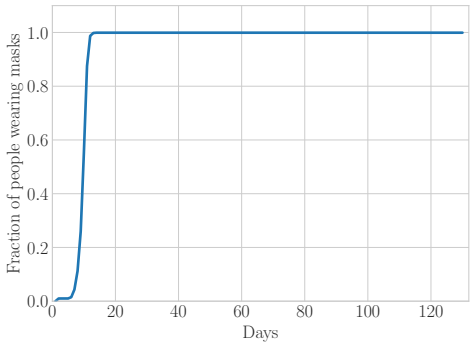


**(b)** Evolution of mask acceptance rate under the first tipping point

**Fig. S19. The co-evolution of the disease and mask adoption at the first tipping points under continued mask mandate.** We fix the transmission probability $p$ of the disease to the value at the first tipping point. Furthermore, we enforce mask mandates when die disease prevalence starts to decrease. Panel $(a)$ shows the infection dynamic, and panel $(b)$ depicts the change in mask adoption percentage. All parameters are set to their baseline values shown in Table S2. Overall, the disease dynamic exhibits only a single wave, and we observe no oscillation of infection and mask adoptions. Furthermore, we sampled a large number of transmission probabilities within the third regime and observed no oscillations. The single-wave dynamics contrast the multiwave dynamics without mask mandate.

## Critical transitions and multiwave infections in a mean-field model

In this section we use a parsimonious mean-field model of disease transmission, coupled with a phenomenological threshold condition approach to model a population's behavioral response. Our goal is to show that the critical transition phenomena of the attack rate are robust to the modeling framework used. That is, we show that the proposed mean-field approach to a well-mixed population can exhibit qualitatively similar results than the proposed multiplex network model.

Consider a population composed of two behaviorally distinct groups: individuals do not complying with precautionary behaviors ($N_1$), and individuals complying with precautionary behaviors ($N_2$), where the total population is given by $N = N_1 + N_2$. Assume the contagion process follows a Susceptible ($S_i$), Infected ($I_i$) and Recovered ($R_i$), structure in each of the behavior groups. Non-compliant susceptible individuals get infected by contacting: $(i)$ non-compliant infected individuals at rate $pS_1\frac{I_1}{N}$, and $(ii)$ compliant infected individuals at rate $pS_1\frac{\sigma_i I_2}{N}$, where $0 \leq \sigma_i \leq 1$ stands for the precautionary efforts of infected compliant individuals. Similarly, compliant susceptible individuals get infected by making contacts with: $(i)$ non-compliant infected individuals at rate $\sigma_s p\frac{I_1}{N}$, and $(ii)$ compliant infected individuals at rate $\sigma_s p\frac{\sigma_i I_2}{N}$, where $\sigma_s$ stands for a reduced susceptibility of compliant susceptible individuals. Infected individuals, regardless of their behavior, recover at rate $\gamma$.

We model *fear of infection* by using a threshold condition based on the disease prevalence level. Non-compliant individuals start following precautionary behaviors after the disease attains a pre-defined prevalence threshold $\tau$. After which, people from the non-compliant group ($N_1$), regardless of their health-status, move to the compliant group ($N_2$) at a rate $\varphi$. Moreover, our fear condition only plays a role whenever the disease prevalence is over the fear threshold ($\varphi > 0$), otherwise there is no recruitment on the compliant populations ($\varphi = 0$). Finally, we assume compliant individuals loss fear of infection and become non-compliant at a rate $\lambda$, regardless of their health-status. The proposed model for behavioral adaptations by a prevalence threshold condition is formalized in the following set

of Ordinary Differential Equations:

$$
\begin{aligned}
\dot{S}_1 &= -(I_1 + \sigma_I I_2) p \frac{S_1}{N} + \lambda S_2 - \varphi S_1, \\
\dot{I}_1 &= (I_1 + \sigma_I I_2) p \frac{S_1}{N} + \lambda I_2 - \gamma I_1 - \varphi I_1, \\
\dot{R}_1 &= \lambda R_2 + \gamma I_1 - \varphi R_1 \\
\dot{S}_2 &= -(I_1 + \sigma_I I_2) \sigma_S p \frac{S_2}{N} - \lambda S_2 + \varphi S_1, \\
\dot{I}_2 &= (I_1 + \sigma_I I_2) \sigma_S p \frac{S_2}{N} - \lambda I_2 - \gamma I_2 + \varphi I_1, \\
\dot{R}_2 &= -\lambda R_2 + \gamma I_2 + \varphi R_1
\end{aligned}
\qquad [A]
$$

where

$$
\begin{aligned}
\dot{N} &= \dot{N}_1 + \dot{N}_2 = 0, \\
\dot{N}_1 &= \lambda N_2 - \varphi N_1, \\
\dot{N}_2 &= -\lambda N_2 + \varphi N_1.
\end{aligned}
\qquad [B]
$$

Notice that $\Omega = \{S_1, I_1, R_1, S_2, I_2, R_2 \in \mathbb{R}^6_+ : S_1 + I_1 + R_1 + S_2 + I_2 + R_2 \leq N\}$, represents a feasible (positively-invariant and attracting) region for the system Eq. (A).

**Results.** Consider an epidemic with $\mathcal{R}_0 = p/\gamma = 2.4$, where $p = 0.48$ and $\gamma = 0.2$. Assume the behavioral response occurs at a threshold prevalence $\tau = 1\%$, after which non-compliant individuals start adopting precautionary behaviors at a rate $\varphi$, and return to non-compliance at a rate $\lambda$. Susceptible (infected) compliant individuals are assumed to reduce their susceptibility (infectiousness) by a factor of $\sigma_i = 0.1$ ($\sigma_s = 0.2$).

Figures S20 and S21 show the evolution of the disease prevalence (panel a) and the epidemic size (panel b) on time. We assume the same disease parameters but different behavioral responses $\varphi = 0.5$ and $\varphi = 0.75$. In S20, we show that even though the disease prevalence is much greater than the fear threshold ($\tau = 0.01$), the population's behavioral response is not fast enough to avoid enough infections during the first epidemic peak ($\varphi = 0.05$). Consequently, the disease prevalence exhibit a big first epidemic peak and a heavy tail, without oscillations.

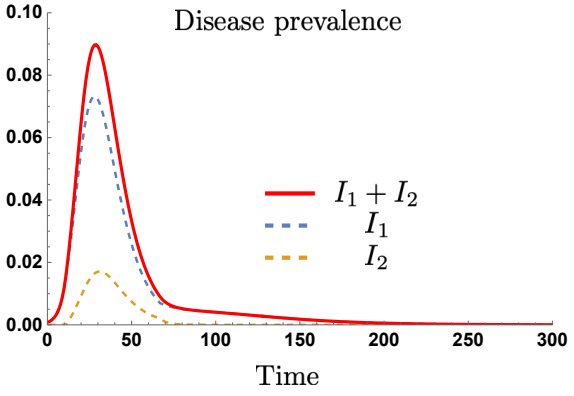


**(a)** Time course of the infected compliant, infected non-compliant, and total disease prevalence.

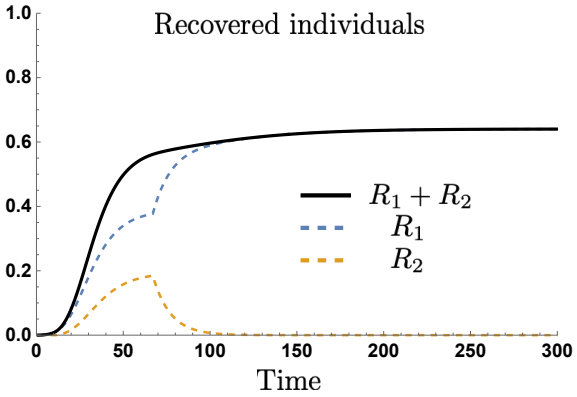


**(b)** Time course of the recovered compliant, non-compliant, and epidemic size.

**Fig. S20. The disease dynamics cross the fear threshold once.** The adoption of precautionary behaviors is not fast enough to maintain an endemic level of compliant individuals. In consequence, the disease prevalence does not show oscillations on the disease prevalence.

In counterpart, S21 show an scenario where, after the disease prevalence hits the fear threshold condition ($\tau = 0.01$), the population comply with precautionary behaviors fast enough ($\varphi = 0.075$), so that the first epidemic peak is highly

reduced. In this scenario, after the disease prevalence is reduced below the fear threshold, not anymore people is recruited on the compliant group ($\varphi = 0$). This produce a resurgence of the epidemic, taking the disease prevalence over the fear threshold again, followed by the population's behavioral response taking the epidemic prevalence down again.

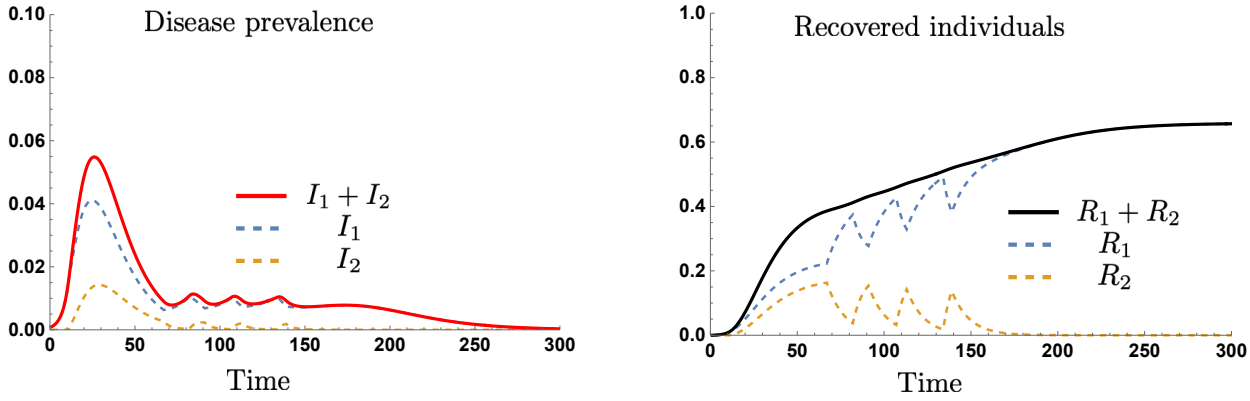


**(a) Fear threshold activate multiple times.** Time course of the compliant, non-compliant, and total disease prevalence.

**(b) Recovered individuals keep changing their behavior.** Time course of the group specific and total recovered individuals

**Fig. S21. The disease dynamics cross the fear threshold multiple times.** The behavioral response rate $\varphi = 0.075$ is enough to produce oscillations on the disease prevalence.

Similar to our network model, the mean-field model captures the trade-off between the strength of the behavioral response (risk reduction), and the disease infectiousness. Whenever there epidemic-behavior dynamics coexist near a balance, the epidemic would survive for long periods, generating secondary cases in the presence/absence of behavioral responses, potentially leading to increased attack rate values.

## Peer-pressure and fear mechanisms in a mean-field model

This section concerns a mean-field model where, as in the main text model, there are two thresholds: a (randomly distributed) fear threshold, $\tau$, and a (randomly distributed) peer-pressure threshold, $\omega$. Our mean-field model is equivalent to assuming a complete network (neighborhood representative of the whole population). Thus, when the disease prevalence is $I$ and the fraction of individuals wearing masks is $m$, we evaluate the fraction of individuals that *want* to wear a mask, $F(I, m)$, as a function of $I$ and $m$. This fraction of the population is made of all of those for which either their fear threshold is lower than $I$ or their peer-pressure threshold is lower than the current $m$. If we let $\rho_\tau(\tau)$ and $\rho_\omega(\omega)$ be, respectively, the probability density distributions of the thresholds $\tau$ and $\omega$, we can write the fraction of individuals that currently want to wear a mask as

$$F(I,m) = \int_{-\infty}^{I} \rho_\tau(\tau)d\tau + \int_{-\infty}^{m} \rho_\omega(\omega)d\omega - \int_{-\infty}^{m}\int_{-\infty}^{I} \rho_\tau(\tau)\rho_\omega(\omega)d\tau d\omega \quad [C]$$

$$= C_\tau(I) + C_\omega(m) - C_\tau(I)C_\omega(m). \quad [D]$$

where we assume the thresholds $\tau$ and $\omega$ are independent and wrote it in terms of the cumulative distributions of the thresholds $\tau$ and $\omega$, $C_\tau(I)$ and $C_\omega(m)$, respectively.

The fraction of mask wearers, $m$ will track this number with some rate $r$, thus,

$$\dot{m} = r(F(I,m) - m). \quad [E]$$

In our case, we consider uniform distributions of thresholds, i.e., $f \sim U(l_\tau, u_\tau)$ and $p \sim U(l_\omega, u_\omega)$. The cumulative

function of these uniform distributions can be written as

$$C_\tau(I) = \frac{I - l_\tau}{u_\tau - l_\tau}\Theta(I - l_\tau) + \frac{u_\tau - I}{u_\tau - l_\tau}\Theta(I - u_\tau), \text{ and} \quad [F]$$

$$C_\omega(m) = \frac{m - l_\omega}{u_\omega - l_\omega}\Theta(m - l_\omega) + \frac{u_\omega - m}{u_\omega - l_\omega}\Theta(m - u_\omega), \quad [G]$$

where we use the Heaviside function $\Theta(x) = \begin{cases} 0 & x \leq 0 \\ 1 & x > 0 \end{cases}$. This allows us to study the sign of $\dot{m}$ as a function of $m$ and $I$.

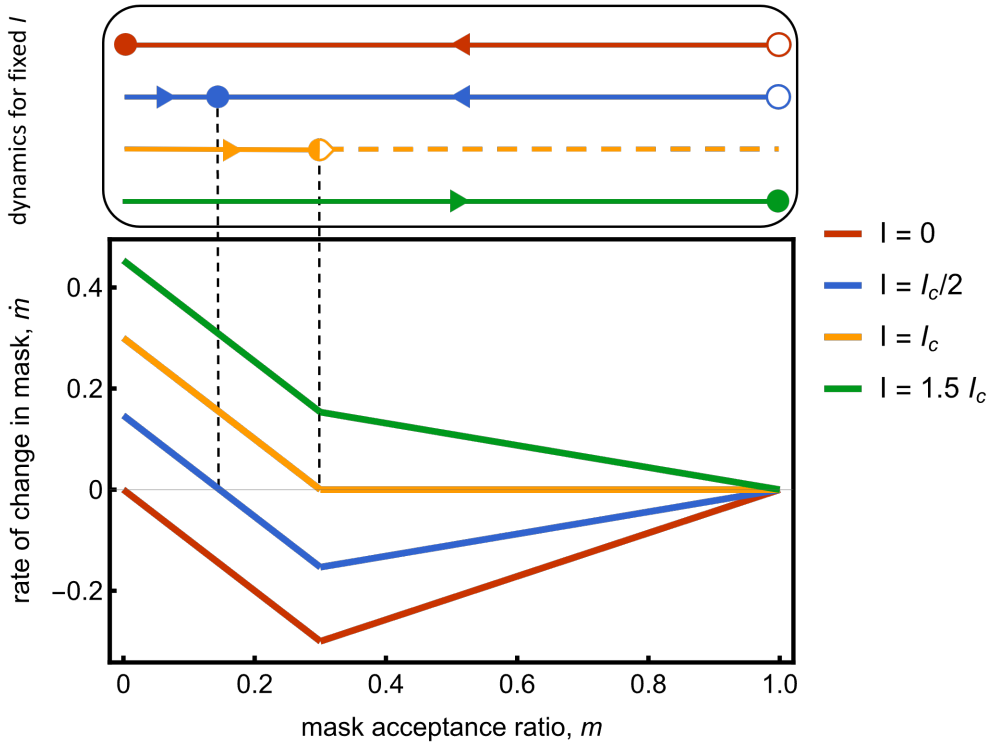


**Fig. S22.** Dynamics of mask wearing for a fixed level of infection ratio, $I$. Full circle represent attractors of the dynamics, whereas open circles represent repellers. For $I < I_c = l_\omega + l_\tau(u_\omega - l_\omega)$ mask wearing tends towards a low value. Above $I_c$, mask wearing tends to 1.

Figure S22 shows the various dynamics for different values of infection ratio, $I$. For a given value of $I$, we can find the value for the fraction of the population wearing a mask, $m^*$, for which mask adoption does not change (full circle at low rates in Figure S22), as a function of the disease prevalence, $I$. We do so by studying the one-dimensional autonomous system in Eq.(E). For $u_\omega = 1$, we get

$$m^*(I) = \begin{cases} 0 & I \leq l_\tau \\ \frac{l_\tau - I}{l_\tau - u_\tau} & l_\tau < I < l_\tau + l_\omega(u_\tau - l_\tau) \\ 1 & I \geq l_\tau + l_\omega(u_\tau - l_\tau) \end{cases} \quad [H]$$

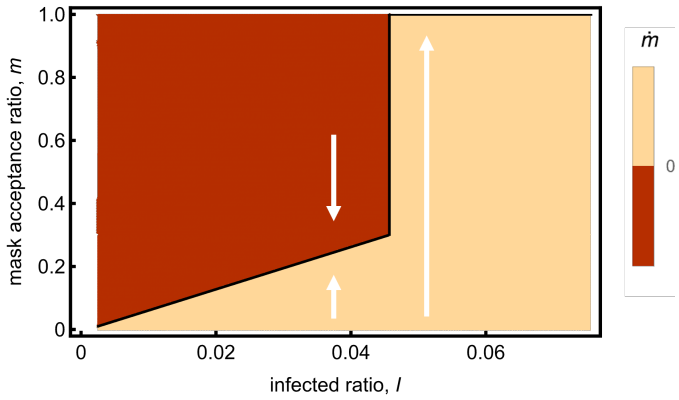


**Fig. S23.** Bifurcation diagram of mask-wearing behavior for infection ratio, $I$, as control parameter. A sharp transition occurs at $I = I_c$.

In Figure S23, we see that as the infected ratio $I$ is below a critical value, mask adoption tends towards a mixed equilibrium (between 0 and 1). As the infected ratio goes above $I_c$, mask adoption grows to 1. For infinite and fully connected networks, the process is reversible.

For the values in the main text, this predicts that mask adoption increases at par with the disease from 0 to about 30% followed by a jump to 100% adoption.

To better classify this transition and relate it to traditional critical transitions theory, we can mollify the threshold distribution to make it infinitely differentiable. We can use a standard mollifier for the uniform distribution (e.g., $e^{\frac{-1}{1-x^2}}$) appropriately shifted and scaled, see below in orange). Notice that this smooth scenario is actually more descriptive of a network setting (as opposed to an infinite well-mixed population) where there is variation in the neighborhoods experienced by the individuals.

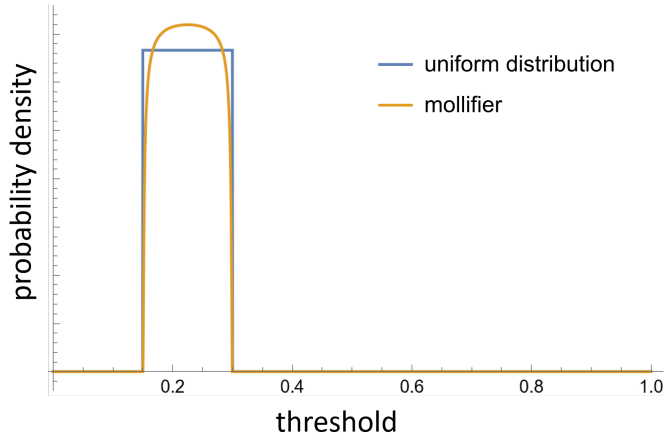


**Fig. S24.** Mollifier for the uniform distributions

Using the mollifier in Figure S24 we obtain the dynamics of Figure S25 and the corresponding bifurcation diagram of Figure S26.

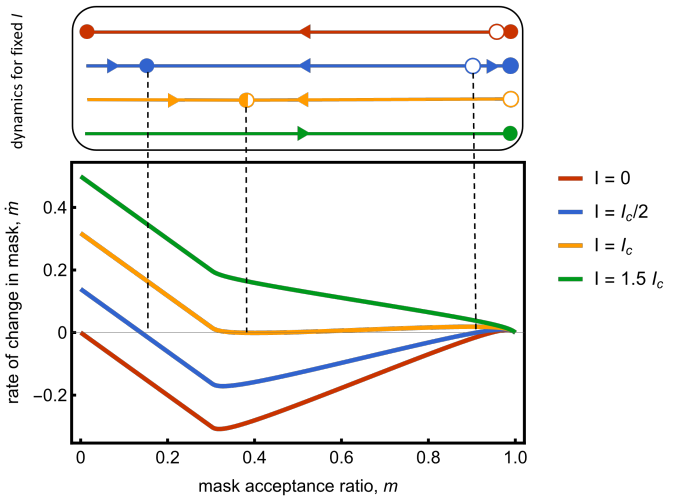


**Fig. S25.** Dynamics for the mollified system in Figure S22 using the distribution represented in Figure S24.

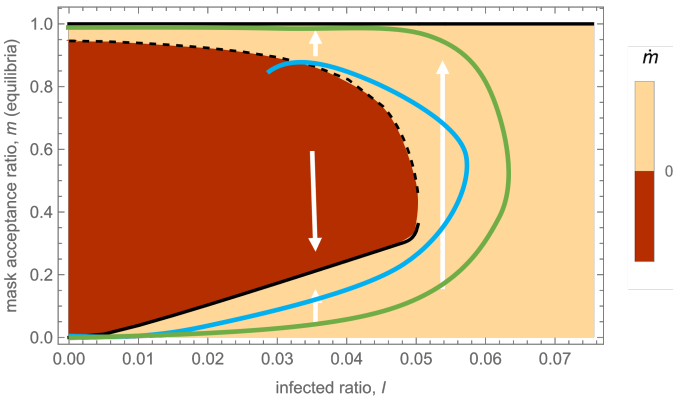


**Fig. S26.** Bifurcation plot for the mollified system in Figure S22 using the distribution represented in Figure S24. Equivalent to the original in Figure S23. In blue and green we illustrate hypothetical (partial) trajectories in the phase plane: one entering the red region that sees mask adoption going down (blue) and another in which the disease drops to zero without having masks rates dropping. Notice that this is not the full phase space since the are also susceptible/recovered states, but the saddle-node region remains constant.

Figure S26 makes it clear that the transition is discontinuous (for an infinite system) and corresponds to a saddle-node bifurcation. It also highlights the hysteresis effect that originates the tipping point.

This bifurcation plot converges to the bifurcation plot for the uniform distribution, since the unstable fixed point moves rapidly towards the top of the plot except for $I = I_c$. For infinite and fully connected populations the process becomes in practice reversible, with any perturbation to $m = 1$ when $I < I_c$ bringing $m$ to $m^* < 1$. Now, we can see what happens at the tipping point by looking at the trajectories in this face plane (illustrated in blue and green). Infection will go up from close to zero to a high value and back, either because mask wearing is high or because the number of susceptibles is low. As the infection ratio increases, mask adoption increases. When infection ratio goes above $I_c$, mask adoption increases abruptly, reducing the increase of the infection ratio. As the infection ration drops, it can do so either by going through the red region or through the yellow region. When it occurs through the red region mask acceptance drops and the cycles repeat while there are enough susceptibles. When it occurs through the yellow region mask wearing remains active until the epidemics is over.

Furthermore, when $u_\omega < 1$, mask adoption shows hysteresis, with $I < l_\tau + l_\omega(u_\tau - l_\tau)$ containing another stable equilibrium at $m^* = 1$. See Luojun Yang et al. (2022) (75) for discussion on variations of this hysteresis phenomenon on mask wearing behavior driven by cultural differences.

We can further describe the dynamics by coupling it with the disease.

Assuming mask behavior does not correlate with disease state, we can couple it with an SIR dynamics to get

$$\dot{S} = -((1-m)I + \sigma_I m I)p(1-m)\frac{S}{N} - ((1-m)I + \sigma_I m I)\sigma_S p\, m\frac{S}{N} \quad [\mathrm{I}]$$

$$\dot{R} = \gamma I \quad [\mathrm{J}]$$

$$\dot{I} = -\dot{S} - \dot{R} \quad [\mathrm{K}]$$

$$\dot{m} = r(F(I,m) - m) \quad [\mathrm{L}]$$

or simply

$$\begin{aligned} \dot{S} &= -\left(1 - m(1-\sigma_I)\right)\left(1 - m(1-\sigma_S)\right) pI\frac{S}{N} \\ \dot{R} &= \gamma I \\ \dot{I} &= -\dot{S} - \dot{R} \\ \dot{m} &= r(F(I,m) - m) \end{aligned} \quad [\mathrm{M}]$$

Figure S27 shows time series of the disease prevalence and mask wearing for model Eq. (M). The selected simulations show the oscillation regime that prolong the epidemic period by oscillations of mask wearing.

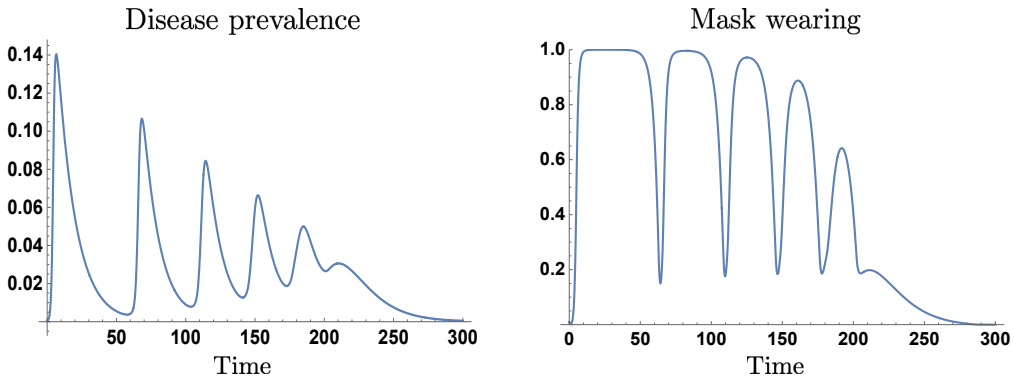


**Fig. S27.** Time course of the disease prevalence and mask wearing. The mask wearings oscillations promotes epidemic reemergence, increasing the attack rate. Parameters identical to main text, with some probabilities now rates. $p = 0.9$, $r = 10$, $\gamma = 1/9$.

Moreover, in Figure S28, our simulations shows that model Eq. (M) also produce a critical transition on the attack rate, similar to the one observed in the network model.

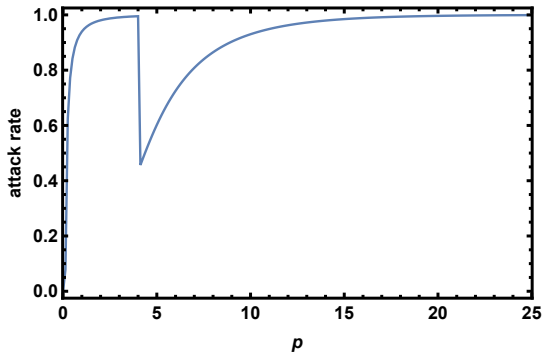


**Fig. S28.** Attack rate for different transmission probabilities $p$. The mean-field model including both behavioral mechanisms shows the critical transition observed in the network model.

## References


1. C Barrett, et al., Predecessor existence problems for finite discrete dynamical systems. *Theor. Comput. Sci.* **386**, 3–37 (2007).
2. M Granovetter, Threshold models of collective behavior. *Am. journal sociology* **83**, 1420–1443 (1978).
3. D Centola, M Macy, Complex contagions and the weakness of long ties. *Am. journal Sociol.* **113**, 702–734 (2007).
4. DJ Watts, SH Strogatz, Collective dynamics of 'small-world'networks. *nature* **393**, 440–442 (1998).
5. ME Newman, ALE Barabási, DJ Watts, *The structure and dynamics of networks.* (Princeton university press), (2006).
6. DJ Watts, A simple model of global cascades on random networks. *Proc. Natl. Acad. Sci.* **99**, 5766–5771 (2002).
7. NA Christakis, JH Fowler, The collective dynamics of smoking in a large social network. *New Engl. journal medicine* **358**, 2249–2258 (2008).
8. D Centola, An experimental study of homophily in the adoption of health behavior. *Science* **334**, 1269–1272 (2011).
9. S González-Bailón, J Borge-Holthoefer, A Rivero, Y Moreno, The dynamics of protest recruitment through an online network. *Sci. reports* **1**, 1–7 (2011).
10. VA Traag, Complex contagion of campaign donations. *PloS one* **11**, e0153539 (2016).
11. D Guilbeault, J Becker, D Centola, Complex contagions: A decade in review. *Complex spreading phenomena social systems* pp. 3–25 (2018).
12. PS Dodds, DJ Watts, Universal behavior in a generalized model of contagion. *Phys. review letters* **92**, 218701 (2004).
13. PS Dodds, DJ Watts, A generalized model of social and biological contagion. *J. theoretical biology* **232**, 587–604 (2005).
14. DJ Watts, PS Dodds, Influentials, networks, and public opinion formation. *J. consumer research* **34**, 441–458 (2007).
15. P Ramazi, J Riehl, M Cao, Networks of conforming or nonconforming individuals tend to reach satisfactory decisions. *Proc. Natl. Acad. Sci.* **113**, 12985–12990 (2016).
16. C Kuhlman, et al., A bi-threshold model of complex contagion and its application to the spread of smoking behavior in *Proceedings of the workshop on social network mining and analysis (SNA-KDD 2011).* (Citeseer), (2011).
17. WM Huang, LJ Zhang, XJ Xu, X Fu, Contagion on complex networks with persuasion. *Sci. reports* **6**, 1–8 (2016).
18. CL Barrett, et al., Complexity of reachability problems for finite discrete dynamical systems. *J. Comput. Syst. Sci.* **72**, 1317–1345 (2006).
19. MO Jackson, Y Zenou, Games on networks in *Handbook of game theory with economic applications.* (Elsevier) Vol. 4, pp. 95–163 (2015).
20. S Hasan, SV Ukkusuri, A threshold model of social contagion process for evacuation decision making. *Transp. research part B: methodological* **45**, 1590–1605 (2011).
21. EM Rogers, A Singhal, MM Quinlan, *Diffusion of innovations.* (Routledge), (2014).
22. J Leskovec, LA Adamic, BA Huberman, The dynamics of viral marketing. *ACM Transactions on Web (TWEB)* **1**, 5–es (2007).
23. F Fu, NA Christakis, JH Fowler, Dueling biological and social contagions. *Sci. reports* **7**, 1–9 (2017).
24. M Salathé, S Bonhoeffer, The effect of opinion clustering on disease outbreaks. *J. The Royal Soc. Interface* **5**, 1505–1508 (2008).
25. E Campbell, M Salathé, Complex social contagion makes networks more vulnerable to disease outbreaks. *Sci. reports* **3**, 1–6 (2013).

26. S Funk, E Gilad, C Watkins, VA Jansen, The spread of awareness and its impact on epidemic outbreaks. *Proc. Natl. Acad. Sci.* **106**, 6872–6877 (2009).
27. C Granell, S Gómez, A Arenas, Dynamical interplay between awareness and epidemic spreading in multiplex networks. *Phys. review letters* **111**, 128701 (2013).
28. S Funk, E Gilad, VA Jansen, Endemic disease, awareness, and local behavioural response. *J. theoretical biology* **264**, 501–509 (2010).
29. L Hébert-Dufresne, D Mistry, BM Althouse, Spread of infectious disease and social awareness as parasitic contagions on clustered networks. *Phys. Rev. Res.* **2**, 033306 (2020).
30. JM Epstein, J Parker, D Cummings, RA Hammond, Coupled contagion dynamics of fear and disease: mathematical and computational explorations. *PLoS One* **3**, e3955 (2008).
31. T Gross, CJD D'Lima, B Blasius, Epidemic dynamics on an adaptive network. *Phys. review letters* **96**, 208701 (2006).
32. G Cencetti, F Battiston, Diffusive behavior of multiplex networks. *New J. Phys.* **21**, 035006 (2019).
33. LG Alvarez-Zuzek, CE La Rocca, JR Iglesias, LA Braunstein, Epidemic spreading in multiplex networks influenced by opinion exchanges on vaccination. *PloS one* **12**, e0186492 (2017).
34. P Jovanovski, I Tomovski, L Kocarev, Modeling the spread of multiple contagions on multilayer networks. *arXiv preprint arXiv:1703.02906* (2017).
35. FM Toxvaerd, Equilibrium social distancing. *Fac. Econ. Univ. Camb.* (2020).
36. F Toxvaerd, Rational disinhibition and externalities in prevention. *Int. Econ. Rev.* **60**, 1737–1755 (2019).
37. DW Berger, KF Herkenhoff, S Mongey, An seir infectious disease model with testing and conditional quarantine, (National Bureau of Economic Research), Technical report (2020).
38. ZA Bethune, A Korinek, Covid-19 infection externalities: Trading off lives vs. livelihoods, (National Bureau of Economic Research), Technical report (2020).
39. PY Geoffard, T Philipson, Rational epidemics and their public control. *Int. economic review* pp. 603–624 (1996).
40. TJ Philipson, RA Posner, , et al., *Private choices and public health: The AIDS epidemic in an economic perspective*. (Harvard University Press), (1993).
41. SE Asch, Opinions and social pressure. *Sci. Am.* **193**, 31–35 (1955).
42. JJ Van Bavel, et al., Using social and behavioural science to support covid-19 pandemic response. *Nat. human behaviour* **4**, 460–471 (2020).
43. SE Bokemper, et al., Beliefs about mask efficacy and the effect of social norms on mask wearing intentions for covid-19 risk reduction. *medRxiv* (2021).
44. FV Hansstein, F Echegaray, Exploring motivations behind pollution-mask use in a sample of young adults in urban china. *Glob. health* **14**, 1–10 (2018).
45. J Barceló, GCH Sheen, Voluntary adoption of social welfare-enhancing behavior: Mask-wearing in spain during the covid-19 outbreak. *PloS one* **15**, e0242764 (2020).
46. M DeJonckheere, M Waselewski, X Amaro, A Frank, KP Chua, Views on covid-19 and use of face coverings among us youth. *J. Adolesc. Heal.* **68**, 873–881 (2021).
47. M Wolf, RH Kurvers, AJ Ward, S Krause, J Krause, Accurate decisions in an uncertain world: collective cognition increases true positives while decreasing false positives. *Proc. Royal Soc. B: Biol. Sci.* **280**, 20122777 (2013).
48. DK Ahorsu, et al., The fear of covid-19 scale: development and initial validation. *Int. journal mental health addiction* pp. 1–9 (2020).
49. A Bendau, et al., Associations between covid-19 related media consumption and symptoms of anxiety, depression and covid-19 related fear in the general population in germany. *Eur. Arch. Psychiatry Clin. Neurosci.* **271**, 283–291 (2021).
50. G Mertens, L Gerritsen, S Duijndam, E Salemink, IM Engelhard, Fear of the coronavirus (covid-19): Predictors

in an online study conducted in march 2020. *J. Anxiety Disord.* **74**, 102258 (2020).
51. L Liu, X Wang, S Tang, H Zheng, Z Zheng, Multilayer social reinforcement induces bistability on multiplex networks. *J. Stat. Mech. Theory Exp.* **2021**, 063402 (2021).
52. KM Fitzpatrick, C Harris, G Drawve, Fear of covid-19 and the mental health consequences in america. *Psychol. trauma: theory, research, practice, policy* (2020).
53. TD Huynh, The more i fear about covid-19, the more i wear medical masks: A survey on risk perception and medical masks uses. *medRxiv* (2020).
54. S Taylor, *The psychology of pandemics: Preparing for the next global outbreak of infectious disease.* (Cambridge Scholars Publishing), (2019).
55. K Nakayachi, T Ozaki, Y Shibata, R Yokoi, Why do japanese people use masks against covid-19, even though masks are unlikely to offer protection from infection? *Front. Psychol.* **11**, 1918 (2020).
56. K Aquino, A Reed II, The self-importance of moral identity. *J. personality social psychology* **83**, 1423 (2002).
57. CH Declerck, C Boone, G Emonds, When do people cooperate? the neuroeconomics of prosocial decision making. *Brain cognition* **81**, 95–117 (2013).
58. J Nai, J Narayanan, I Hernandez, K Savani, People in more racially diverse neighborhoods are more prosocial. *J. Pers. Soc. Psychol.* **114**, 497 (2018).
59. L He, et al., Why do people oppose mask wearing? a comprehensive analysis of us tweets during the covid-19 pandemic. *PubMed* (2021).
60. LH Kahane, Politicizing the mask: Political, economic and demographic factors affecting mask wearing behavior in the usa. *East. economic journal* **47**, 163–183 (2021).
61. NC Brienen, A Timen, J Wallinga, JE Van Steenbergen, PF Teunis, The effect of mask use on the spread of influenza during a pandemic. *Risk Analysis: An Int. J.* **30**, 1210–1218 (2010).
62. NH Leung, et al., Respiratory virus shedding in exhaled breath and efficacy of face masks. *Nat. medicine* **26**, 676–680 (2020).
63. SE Eikenberry, et al., To mask or not to mask: Modeling the potential for face mask use by the general public to curtail the covid-19 pandemic. *Infect. Dis. Model.* **5**, 293–308 (2020).
64. RB Patel, SD Skaria, MM Mansour, GC Smaldone, Respiratory source control using a surgical mask: an in vitro study. *J. occupational environmental hygiene* **13**, 569–576 (2016).
65. KT Diaz, GC Smaldone, Quantifying exposure risk: surgical masks and respirators. *Am. journal infection control* **38**, 501–508 (2010).
66. B Espinoza, M Marathe, S Swarup, M Thakur, Asymptomatic individuals can increase the final epidemic size under adaptive human behavior. *Sci. reports* **11**, 1–12 (2021).
67. R Wölfel, et al., Virological assessment of hospitalized patients with covid-2019. *Nature* **581**, 465–469 (2020).
68. EJ Van Leeuwen, DB Haun, Conformity without majority? the case for demarcating social from majority influences. *Animal Behav.* **96**, 187–194 (2014).
69. A Millie, *Anti-social behaviour.* (McGraw-Hill Education (UK)), (2008).
70. CR MacIntyre, et al., The efficacy of medical masks and respirators against respiratory infection in healthcare workers. *Influ. other respiratory viruses* **11**, 511–517 (2017).
71. J Chen, et al., Prioritizing allocation of covid-19 vaccines based on social contacts increases vaccination effectiveness. *medRxiv* (2021).
72. S Eubank, et al., Modelling disease outbreaks in realistic urban social networks. *Nature* **429**, 180–184 (2004).
73. CL Barrett, et al., Generation and analysis of large synthetic social contact networks in *Proceedings of the 2009 Winter Simulation Conference (WSC).* (IEEE), pp. 1003–1014 (2009).
74. HS Mortveit, et al., Synthetic populations and interaction networks for the U.S., (NSSAC, University of Virginia), Technical report (2020).

75. L Yang, et al., Socio-cultural determinants of global mask-wearing behavior. Available at SSRN: https://ssrn.com/abstract=4024271 (2022).